



1 **Imaging of the active root current pathway under partial root-zone drying** 2 **stress: A laboratory study for *Vitis vinifera*.**

3 Benjamin Mary^{1,2}, Veronika Iván¹, Franco Meggio^{3,4}, Luca Peruzzo^{1,2}, Guillaume Blanchy⁵, Chunwei
4 Chou², Benedetto Ruperti^{3,4}, Yuxin Wu², Giorgio Cassiani¹

5 ¹Dipartimento di Geoscienze, Università degli Studi di Padova, Padova, Italy

6 ²Earth and Environmental Sciences Area, Lawrence Berkeley National Laboratory, California, USA

7 ³Department of Agronomy, Food, Natural resources, Animals and Environment – DAFNAE, University of Padova, Agripolis,
8 Viale dell'Università 16 – Legnaro (Padova), Italy;

9 ⁴Interdepartmental Research Centre for Viticulture and Enology - CIRVE, University of Padova, Via XXVIII Aprile 14,
10 Conegliano (Treviso), Italy;

11 ⁵Urban and Environmental Engineering, University of Liège (ULiege), Liège, Belgium

12

13 *Correspondence to:* B. Mary (benjamin.mary@unipd.it)

14

15 **Abstract**

16 Understanding root signals and their consequences on the whole plant physiology is one of the keys to tackling the water-
17 saving challenge in agriculture. The partial root-zone drying (PRD) method is part of an ensemble of irrigation strategies that
18 aim at improving water use efficiency. To reach this goal tools are needed for the evaluation of the root's and soil water
19 dynamics in time and space. In controlled laboratory conditions, using a rhizotron built for geoelectrical tomography imaging,
20 we monitored the spatio-temporal changes in soil electrical resistivity for more than a month corresponding to six Partial
21 Rootzone Drying (PRD) cycles. Electrical Resistivity Tomography (ERT) was complemented with Electrical Current Imaging
22 (ECI) using plant stem-induced electrical stimulation. We demonstrated that under mild water stress conditions, it is practically
23 impossible to spatially distinguish the PRD effects using ECI. We evidenced that the Current Source leakage depth varied
24 during the course of the experiment but without any significant relationship to the soil water content changes or transpiration



25 demand. On the other hand, ERT showed spatial patterns associated with irrigation and, to a lesser degree, to RWU. The
26 interpretation of the geoelectrical imaging with respect to root activity was strengthened and correlated with indirect
27 observations of the plant transpiration using a weight monitoring lysimeter and direct observation of the plant leaf gas
28 exchanges.

29 **1. Introduction**

30 In the context of water scarcity, agriculture needs to improve irrigation practices by reducing water inputs and selecting
31 adequate species and, in the case of woody crops, most efficient scion-rootstock combinations. In order to evaluate the efficacy
32 of irrigation, it is necessary to develop tools capable of evaluating root functioning and quantifying root water uptake. The
33 partial root zone drying (PRD) method is part of an ensemble of irrigation strategies that aim at improving water use efficiency.
34 It consists of irrigating only one part of the root system of the same plant using a certain percentage of the potential
35 evapotranspiration (ET_p), usually inferior to the total water needed. Application of PRD triggers a physiological response in
36 the plant via a hormone called Abscisic acid (ABA), which is produced in the roots and transmitted to the leaves to regulate
37 the stomata closure and thus reducing water transpiration while keeping photosynthesis active and finally leading to increased
38 water use efficiency. A number of publications investigated the origins of the mechanism controlling transpiration during PRD
39 (Stoll et al., 2000), while others focused on the consequences in terms of Root Water Uptake (RWU) and production crop
40 yield (Collins et al., 2009).

41 The plant's natural bioelectrical activity is necessary for its physiological processes. Plant scientists represent it by a water
42 column where the ions move from bottom to top and vice versa due to gradients of water potentials. In their studies, Voytek
43 et al. (2019) and Gibert et al. (2006) successfully linked the measurements of electrical potential in the ground and in the tree
44 stem to the RWU and sap flow respectively. The use of active methods such as electrical resistivity tomography (ERT) allows
45 for spatial and temporal analysis of the subsoil. Recent advances in electrical tomography imaging, in particular reduced at the
46 plant scale, show their effectiveness to measure changes in soil water content associated with the RWU (e.g. Cassiani et al.,
47 2015, 2016; Mary et al., 2018). Applications of geoelectrical methods to evaluate water use efficiency are increasing. Recently



48 in an experimental Citrus orchard, Consoli et al., (2017), Vanella et al., 2018 and Mary et al., (2019a) showed that soil moisture
49 patterns determined by PRD are visible from the ERT perspective and can be attributed to the root system distribution.

50 However, processes occurring in the rhizosphere can affect the soil electrical resistivity (ER) in various ways. Roots induce
51 changes in the soil structure in terms of porosity and hydraulic conductivity which ultimately modify the water pathways and
52 fluxes and thus the ER itself. Stemflow channelling by roots is an example of how water from rain or irrigation can be driven
53 to soil recharge by the root structure. Conversely, root uplift in agroforestry shows how water can move from the deeper layers
54 to the top via the roots.

55 Roots also affect the soil ER through the geochemical changes associated with root exudates and root symbiosis. At the
56 interface between soil and roots, the chemical gradients and concentrations can drastically differ from those observed in the
57 soil regions not affected by the roots. Although this can have a significant impact and be a valuable source of information,
58 only a few studies have extended the ERT and the induced polarisation (IP) to observe these changes (Weigand, 2017; Weigand
59 and Kemna, 2019; Tsukanov and Schwartz, 2020, 2021). As of today, the electrical behaviour of individual roots remains
60 poorly understood, particularly with regard to their changes in type (from hair roots to fully lignified roots), space, time, and
61 whether the root is active or not (Ehosioko et al., 2020).

62 The geophysical approach extends the scope of traditional methods to evaluate soil water content (SWC) using time-domain
63 reflectometry (TDR) sensors and the calculation of RWU (Jackisch et al., 2020). In the field, the spatial resolution is controlled
64 (in ERT or IP) by the arrangement of the electrodes and acquisition parameters (Uhlemann et al., 2018), while the temporal
65 resolution is controlled by the time it takes to complete a full sequence measurement.

66 Rhizotrons are one of the earliest and most effective tools for studying root growth and functioning, both in the field and in
67 the laboratory (Taylor et al., 1990). They are transparent boxes that allow the direct observation of the roots during plant
68 growth and changes in soil conditions. Rhizotrons also provide valuable support in multidisciplinary studies, allowing other
69 methods to be more easily and precisely deployed, so that their results more reliably interpreted. For example, a load scale is
70 often mounted in combination with the rhizotron in order to weigh the system, which allows inferring the quantity of water
71 lost by the plant over time. This set-up is inspired by the lysimeter and is widely adopted to measure the water balance of the



72 soil-plant interactions. For example, in a rhizotron, Doussan and Garrigues (2019) use the light transmission 2D technique to
73 infer root water uptake with respect to their genotypes.
74 The very few studies conducting geophysical tomography imaging in the laboratory using a rhizotron proved a certain
75 efficiency in studying the interaction between soil physics and plant physiology for predicting plant response to environmental
76 stresses (Weigand, 2017, 2019; Peruzzo et al., 2020). It allows for high-resolution tomography by reducing the size, diameter,
77 and spacing of the electrodes. The entire soil profile is easily accessible by placing electrodes on the side of the rhizotron,
78 easing the depth resolution limitation inherent to surface-based geophysical methods usually used for field acquisition.
79 Although there is a good momentum for the use of geophysical methods applied to agronomy (Garré et al., 2021), a number
80 of gaps still need to be addressed. All the indirect root effects on the soil ER affect the evaluation of the soil water content,
81 making the interpretation of ERT to quantify RWU sometimes difficult (Ehosioko et al., 2020).

82 **1.1. Current pathways in roots under PRD constraints**

83 Current pathways in roots remain certainly the main unknown since there is a gap in techniques to measure
84 it non-destructively (Ehosioko et al., 2020; Liu et al., 2021). The current pathways in roots are possibly
85 linked to RWU. Lovisolo et al. (2016) describe in detail the flow of water from root water uptake and the
86 processes occurring at the cell scale. In any case, root water uptake is not distributed equally over the whole
87 root system, due to in part of heterogeneous soil conditions. For the same reason as soil saturation can change
88 over time, RWU is also varying in the time. For active roots, root water uptake consists in a moving water
89 from the root tip (which is usually much more electrically conductive due to high water conductivity at its
90 proximity) in the radial direction via cellular (symplastic way) and between cells (appoplastic way) until it
91 reaches the xylem which transport it in the axial direction towards the upper part. Water flow can encounter
92 resistances due to suberization (conversion of the cell walls into cork tissue by development of suberin),
93 which is naturally driven as a consequence of root growth (secondary roots are more suberised than primary
94 roots) but it can also be the consequence of plant stress (Malavasi et al., 2016; Song et al., 2019). The process
95 can cause reductions in water conductivity through the root system by limiting the permeability of the root
96 tissue, thus leading to changes in the plant's ability to take up water. For the specific PRD case, there is a



97 complex balance between reducing radial flow (as a consequence of ABA signalling sent by the roots) to
98 conserve water in the soil but keeping the axial flow active. This can be done for instance by adjusting the
99 xylem vessels size and quantities. Although suberisation is usually a long-term process, studies show that
100 PRD can promote and accelerate the process of suberization in response to water limitation. Finally during
101 PRD conditions we can also observe transfer of water from the wet to the dry side through the roots
102 (overnight) in a process called redistribution (Yan et al., 2020), which induces spatio-temporal variations in
103 RWU that ultimately influences also electrical current pathways in roots.

104 A direct approach to analysing the active part of the root system consists of an injection of current stimuli
105 into the plant stem. The so-called “capacitance approach” has been developed for years by plant
106 physiologists, starting from the theory developed by Dalton (1995) who conceptualized the current pathways
107 through the root xylem by an equivalent parallel resistance-capacitance circuit. The theory holds under the
108 assumption that the current flows throughout the most conductive path and is held (thus inducing
109 polarization) by the root cell membranes before being released into the soil. Since then, contrasted
110 experimental results opposed on the relationship between root capacitance (“EC_{root}”) and root traits in
111 various crops, particularly because of studies supporting the major contribution of the stem compared to the
112 roots on the total EC_{root} measured and the possible current leakage at the proximal part (Urban et al., 2011;
113 Dietrich et al., 2018; Peruzzo et al., 2020).

114 Without being able yet to give hints about the electrical current pathway, recent advancements in the
115 development of explicit RWU models, based on plant hydraulics, provide insights into how robust
116 capacitance models hold and under which conditions. We learnt, for instance, that at the root level, RWU
117 models account for the anisotropy by separating the root hydraulic conductance into two terms (longitudinal
118 and radial). The same applies to the stem-based methods as root hydraulic conductance and electrical
119 conductivity are likely to vary conjointly. Up to now the relationship between root water content and root
120 hydraulic conductivity with electrical resistivity has not been firmly established. Many other parameters can
121 affect the water flow as well as the current pathway of stem-based methods.



122 Peruzzo et al. (2020) hypothesize that drought stress can also reduce electrical current leakage, particularly
123 for woody species. Furthermore, as expected, the frequency of the injected current plays an important role
124 in the capacitance measured. At high frequencies, both the longitudinal conductivity and radial conductivity
125 increase (Mancuso 2012; Ehosioke et al. 2020), which can also cause current leakage problems (Gu et al.,
126 2021). The measure of plant responses over multiple frequencies, a method called Electrical Impedance
127 Spectroscopy (EIS) is more time-consuming but more informative since different polarisation processes can
128 manifest themselves in the signal (Ehosioke et al., 2020). The contrast of electrical resistivities between soil
129 and roots plays a fundamental role as reported e.g. by Cseresnyés et al. (2020). Gu et al. (2021) stated that
130 the potential to directly quantify root traits under dry conditions is higher than under wet conditions and
131 interpreted this as a result of the fact that the root electrical longitudinal conductivity is higher than that of
132 the soil under dry conditions. The instrumentation and acquisition schemes used for EC are also questionable
133 and the optimal experimental setup of measurement remains to be determined (Postic and Doussan, 2016).
134 The number and the position of the stem and the return electrodes are a cause of uncertainties (electrode
135 contact resistance, etc.). Peruzzo et al. (2021), in a three channels experiment, were able to provide direct
136 access to the response of stem and soil, which ultimately allowed the decoupling of the root response.
137 Evidence showed the presence of current leakage in herbaceous root systems, a significant contribution from
138 plant stem, and a minor impact from the soil.

139 Gu et al. (2021) stated that in addition to the traditional regression model used for predicting root traits using
140 the EC method, a forward model would help to illustrate the importance of these different factors. In order
141 to cope with the main drawbacks of the EC methods, we propose the so-called Electrical Current Imaging
142 (ECI) method, a physically based approach based on recovering the current density distribution instead of
143 simply calculating the total resistance/capacitance. This method is also referred to as *mise-à-la-masse*
144 (MALM) in the applied geophysics literature. The current imaging methods hold some promise to offer a
145 first set of evidence about the current pathways: This is a popular technique adopted e.g. by the neurosciences
146 community, where the current density in the human brain correlates with diverse patterns of neural activity



147 (Kamarajan et al., 2015). Peruzzo et al. (2020) applied it for plant roots imaging with relative success, as the
148 authors stated that all the current leaks at the plant's proximal part i.e. at the shallowest contact of the plant
149 stem with the soil. For the ECI approach, the Poisson's equation serves as a physical model for the electrical
150 current flow. As current flow is modulated by the conductivity of the soil, the ECI approach is always
151 combined with ERT in order to recover of the soil resistivity distribution.

152 1.2. Study aims and assumptions

153
154 The aim of this study is twofold:

- 155 (i) we aim at showing that the current path through the root system is linked to the active root zones.
156 (ii) we want to investigate how the soil water content affects the current path.

157 For this, we rely on the following assumptions:

- 158 - changes in soil water content measured by ERT are a relevant spatial
159 proxy of root activity and can be used as an indicator of the actual plant
160 transpiration by correlating them with variations of the total rhizotron
161 measured weight.
162 - during the application of PRD, only one part of the root system would
163 be active and the current injected in the stem would preferably spread
164 to the side where the root system is irrigated.

165
166
167

168 2. Material and methods

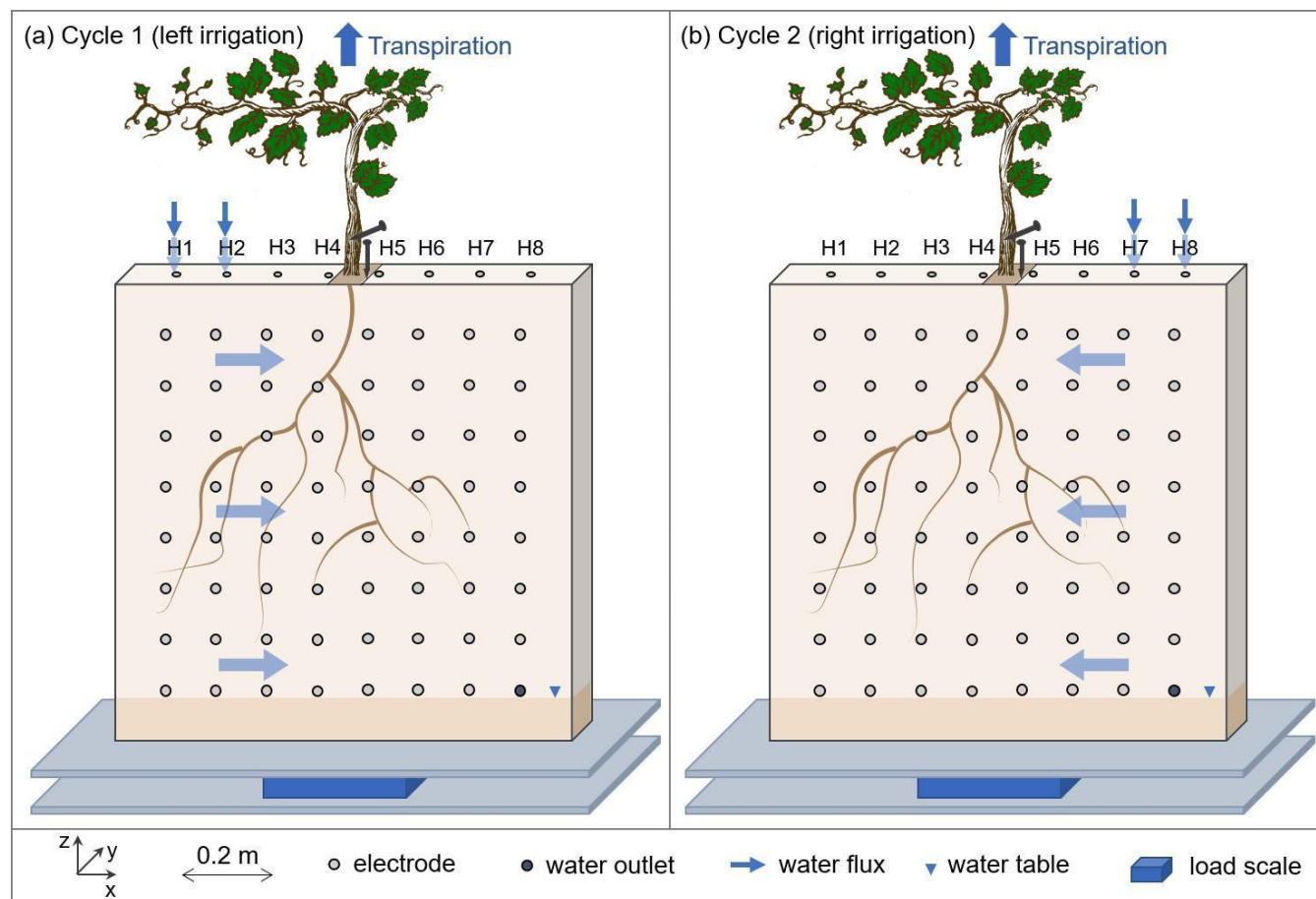
169



170 **2.1. Experimental setup**

171 **2.1.1. Rhizotron**

172 The experiment was conducted using a rhizotron 50 cm wide, 50 cm high, and 3 cm thick, with a
173 transparent screening face. The front of the rhizotron was equipped with 64 stainless steel electrodes
174 with 4 mm diameter which did not extend into the rhizotron's inner volume (Fig. 1). An additional
175 line on the top surface of the rhizotron was composed of 8 electrodes inserted to 1 cm depth. A
176 growth lamp was installed above the rhizotron and turned on during daylight hours (from 7 am to
177 7 pm). The rhizotron was closed on all sides and watertight, with only 8 small holes used for the
178 irrigation at the surface and the central hole where the plant is placed. We considered the surface
179 of these holes to be sufficiently small to neglect the possible effect of evaporation through them.
180 An outlet point was placed on the bottom right side ($z=5\text{cm}$) and the rhizotron was always saturated
181 below this point. In the course of the experiment (after the growing period) no water discharge was
182 observed through the outlet point.



183

184

185

186

187

188

Figure 1: Conceptual figure showing the position of the plant in the rhizotron. The water input was done alternatively from left (a) to right (b) via small holes on the top of the rhizotron (H1 to H8). The roots are free to grow on both sides of the rhizotron. The circles on the screening face show the locations of the electrodes. Two additional electrodes (needles) are used for the ECI, one for the stem injection and the other for the control soil injection next to the stem. The rhizotron is weighted by a central point load scale (PC60-30KG-C3, Flintec) mounted between two support plates in plexiglass.

189

2.1.2. Plant treatment

190

191

192

193

194

195

196

At the initial stage of the experiment, we used a *Vitis Vinifera* cutting with a pre-developed root system (rooted cutting var. Merlot) was used. The cutting was grown in hydroponic solution (modified Hoagland medium) for 4 months before being transferred into the rhizotron. This was followed by a growing period of 5 weeks with irrigation applied over the whole width of the rhizotron every 3 days. The vine was then irrigated with a nutrient solution (see Table 1) following a PRD protocol.



2.1.3. Soil type

The experiment was conducted in a sand-peat mixture (50-50 m/m%). The applied sand was high-purity quartz sand ($\text{SiO}_2 = 99\%$) of grain size comprised between 0.1-0.6 mm and the peat was a normal commercial acidic sphagnum peat. During the course of the experiment, the soil was stable through time with very low compaction (1 cm) observed at the end of the experiment (already observed by Doussan & Garrigues, (2019) for soil with a lower density than 1.5-1.6 g/cm^3). The sand-peat mixture was chosen as a compromise between water retention and drainage. We estimated the porosity at the beginning of the experiment as equal to 55% using the ratio of water weight after saturation to the total volume of the rhizotron.

2.1.4. Irrigation schedule

For each irrigation we regulated the amount of water supplied based on the information obtained from the scale data, the plant received 75% of the measured transpiration. For each cycle, the wetting side changed (from left to right). Note that in this experiment, we did not consider a physical barrier to separate the two sides of the rhizotrons to a split-roots configuration as is the case for other PRD experiments conducted in the laboratory (Martin-Vertedor and Dodd, 2011; Sartoni et al., 2015). In general, the use of physical barriers in Partial Root Zone Drying (PRD) experiments is not always a standard aspect of the setup.

Table 1 describes all cycles conducted from April 13 to July 07:

- The goal of Cycle number -1 was to ensure plant adaptation and growth after transplantation.
- Cycle numbers 0 to 2 aimed at starting the PRD irrigation with half of the rhizotron volume irrigated; i.e. we irrigated the side through a total of four holes out of eight (see Fig. 1).
- From cycle number 3 to 9, we restricted the water input only to the two lateral holes.
- Between cycles 3 and 4, we added intermediate irrigation on the full length of the rhizotron.



222 For the irrigation, we used a nutrient solution (modified Hoagland) (Hoagland and Arnon, 1950)
223 having an electrical conductivity equal to $2470 \pm 5 \mu\text{S/cm}$ (at $\sim 25^\circ\text{C}$), except for cycle 3 where tap
224 water was used ($560 \mu\text{S/cm}$).

225
226

Date (YYYY-mm-dd)	Hole (H) location (c.f. Fig. 1)	Quantity (mL)*	Cycle nb
2022-05-13	All		-1
2022-05-19	H1;H2;H3;H4	200	0
2022-05-25	H5;H6;H7;H8	260	1
2022-05-01	H1;H2;H3;H4	290	2
2022-06-08	H7;H8	305	3
2022-06-10	All	60	- (<i>3bis</i>)
2022-06-15	H1;H2	350	4
2022-06-22	H7;H8	375	5
2022-06-29	H1;H2	386	6
2022-07-05	H7;H8	431	7
2022-07-11	H1;H2	431	8
2022-07-12	H1-H8	200	9

227
228 **Table 1: Irrigation log, indicating the date, the location where the water was input and the**
229 **corresponding cycle number considered in the results. Colors correspond to the side used for the**
230 **irrigation, green is on the right side while orange is on the left side. * Quantity in total distributed over**
231 **all the holes.**

232 2.2. Electrical Resistivity Tomography

233 Electrical Resistivity Tomography consists in reconstructing the subsoil electrical resistivity using an array
234 of electrodes (Binley and Slater, 2020). In this study, a total of 72 stainless steel electrodes were used, 64



235 electrodes formed a grid, 5 cm spaced, covering the screening face of the rhizotron, and an additional line of
236 8 electrodes was posed at the top surface. Electrodes are needles 4 mm in diameter and 80 mm in length, but
237 only their tip is in contact with the soil. ERT involves the measurement of transfer resistances following a
238 sequence describing a combination of varying injections (AB) and potential (MN) pairs of the electrodes.
239 We used a custom sequence composed of 4968 quadrupoles including the reciprocals (e.g. Parsekian et al.,
240 2017), and the measurement were conducted using a Syscal Pro (Iris Instrument) resistivity meter., The
241 sequence was optimized over the ten physical channels of the instrument in order to reduce the acquisition
242 time to approximately 30 min. The data acquisition parameters were constant along the monitoring, with a
243 minimum required V_p of 50 mV, a maximum injection voltage V_{AB} of 50 V, and a number of 3-6 stacks with
244 the on-time fixed to 250 ms each.

245 **2.3. Electrical Current Imaging**

246 The electrical current imaging (or *Mise-à-la-masse*) method was logistically similar to ERT. The sequence
247 nevertheless varies, as the pairs of injection electrodes were kept constant with the positive pole (+I)
248 electrode located on the stem, and the return (-I) electrode located in the bottom right of the rhizotron. The
249 potential electrodes pairs (MN) vary according to a custom sequence. For the stem current stimulation, we
250 inserted a small stainless steel needle (2 cm, 1 mm diameter) into the plant stem at 5 cm from the grafted
251 point. The needle was inserted all the way to the centre of the stem (Fig. 1). Before each measurement, we
252 added a few drops of water to the stem needle in order to reduce the stem contact resistance (to values
253 comprised between 41 and 66 k Ω). The current was guided to the root system via the stem and then released
254 into the soil.

255 As the effect of the stem contact resistance affects the measured voltage, a control soil injection was
256 systematically made. In that case, the current was injected into the soil close to the plant (Fig. 1). A
257 qualitative comparison between the control soil injection and the stem injection plant could be made to
258 discriminate the effect of roots. Furthermore, soil control injection served as a visual calibration for the
259 inversion of the current source knowing that the injection is punctual and occurs at a known position.



260

261

2.4. Weight monitoring for the estimation of transpiration

262

263

264

265

266

267

268

In order to track the weight changes due to the transpiration of the plant, the rhizotron was equipped with a single point load cell (PC60-30KG-C3, Flintec), mounted between two plates in plexiglass supporting the rhizotron (Fig. 1). The data were logged with a sampling rate of 5 min using the weight indicator DAD-141.1. The total weight of the rhizotron is about 20 kg and the expected resolution according to the sensor datasheet is 0.1 g. The variation due to temperature was monitored, on average in May at 22°C, and in July at 25°C. To avoid sharp signal perturbation, during the irrigation and the acquisition of geophysical data the logger was paused.

269

2.5. Leaf gas exchange observations

270

271

272

273

274

275

276

277

278

279

280

281

282

In order to monitor the physiological response of the plant during the course of the experiment, stomatal conductance to water (g_{sw} [$\text{mmol H}_2\text{O m}^{-2} \text{s}^{-1}$]) measurements were performed on vine leaves with an open flow-through differential porometer (LI-600, Li-Cor Inc., Lincoln, Nebraska, USA). The stomatal conductance is a measure of the density, size, and degree of opening of the stomata, therefore it can be used as an indicator of plant water status (Gimenez et al., 2005). The measurements were carried out on 26 leaves in the morning hours (at 10 a.m.), once (on 8th June 2022) just before irrigation (severe water stress), and once (on June 16, 2022) one day after irrigation (mild to low water stress). For the tracking of the plant development, the length (L) and the width (W) of every leaf were measured every 2 weeks from the beginning of the growing period until the end of the experiment. From this data the total leaf area (LA) was estimated according to three models: $LA1 = 0.587 (L \times W)$ (Tsialtas et al., 2008); $LA2 = -3.01 + 0.85 (L \times W)$ (Elsner and Jubb, 1988); $LA3 = -1.41 + 0.527W^2 + 0.254L^2$ (Elsner and Jubb, 1988).



2.6. Data processing

2.6.1. Analysis of ERT data

The ERT acquisition sequence was initially tested on the rhizotron filled with water of known conductivity and it offered good coverage on most of the rhizotron surface with a slight decrease on the sides. The soil electrode contact resistances varied over the course of the experiment between 5 and 20 k Ω . Data were filtered on the basis of the percentage of variations between direct and reciprocal measurements. We chose to eliminate the data with reciprocal relative errors larger than 5%, for all the time steps. The number of rejected data varies from 9% to 39 % of the total (see Table A1) with a median of 11%. Transfer resistances were inverted using the open-source code ResIPy (Blanchy et al., 2020) based on the Fortran R3t code (Binley, 2015). The inversion mesh is an unstructured grid composed of tetrahedra, created using Gmsh (Geuzaine and Remacle, 2009). Two distinct strategies can be used: (1) individual inversion which consists of building a model of resistivity at a given time, and (2) time-lapse inversion (difference inversion) where the difference in resistivity is inverted between a given survey and a background survey (in this case, the background survey is the previous one). In this study, we used the second approach, which allowed filtering of systematic noise and highlights variations (as a percentage of differences) between two times.

2.6.2. Analysis of current density

The mathematical formulation for the inversion of the current source density (ICSD) has been developed in previous studies. It consists in searching for a linear combination of Ohm's law, for a series of current punctual sources (also called virtual sources) minimizing the misfit between simulated and observed data. The algorithm was initially tested on the rhizotron filled with water of known electrical conductivity and a single isolated cable (see the procedure from Peruzzo et al., 2020). It is important to note that the ICSD relies on the knowledge of the medium conductivity (as in the Poisson's equation, the current is modulated by the electrical conductivity). Thus, we used



308 the inverted ER values as the resistivity distribution for the forward modelling in the current density
309 inversion. As for ERT, choices must be made on how data and models are weighted and regularised
310 during the inversion. In this study, we run unconstrained (no prior information) inversions for all
311 the time steps with a regularisation (smoothing using the first derivative). The numerical routine
312 includes a “pareto” functionality wherein regularization and model-to-measurement fit are traded
313 off to estimate the optimum regularization weight w_r . The code used for this inversion is available
314 at <https://github.com/Peruz/icsd>.

315 2.6.3. Calibration of petrophysical relationships

316 In order to estimate the soil water content in the rhizotron during the experiment, we needed to
317 adopt a suitable constitutive model, starting from the available electrical resistivity measurements.
318 Archie's (1942) law (eq. 1) is a widely used empirical relationship that relates the electrical
319 resistivity (ρ) of a bulk material to its porosity (Φ), the contained fluid (water) electrical resistivity
320 (ρ_f) and the fluid saturation (S). Archie's parameters a , m , and n are empirically derived, generally
321 named as follows: a is the tortuosity factor, m is the cementation exponent and n is the saturation
322 exponent.

$$\rho = a \rho_f \Phi^{-m} S^{-n} \quad (1)$$

323 We calibrated these parameters experimentally, as usually done, by collecting water saturation-ER
324 values over different soil samples. The sample holder (a cylinder of 150 mm inner height and 41
325 mm inner diameter) allows for a four-point measurement of the ER converted to apparent electrical
326 resistivity using the appropriate geometrical factor. The adopted water electrical conductivity is
327 known and fixed ($594 \mu\text{S}/\text{cm}$ at $\sim 25^\circ\text{C}$). Porosity was assumed to be equal to 0.55, which is the
328 same of the soil mixture in the rhizotron. The sample was initially saturated to field capacity and
329 progressively desaturated. The field capacity was estimated by gravimetric method approximately
330 at 40% of volumetric water content (m^3/m^3). In total, 6 measurements were collected at respectively



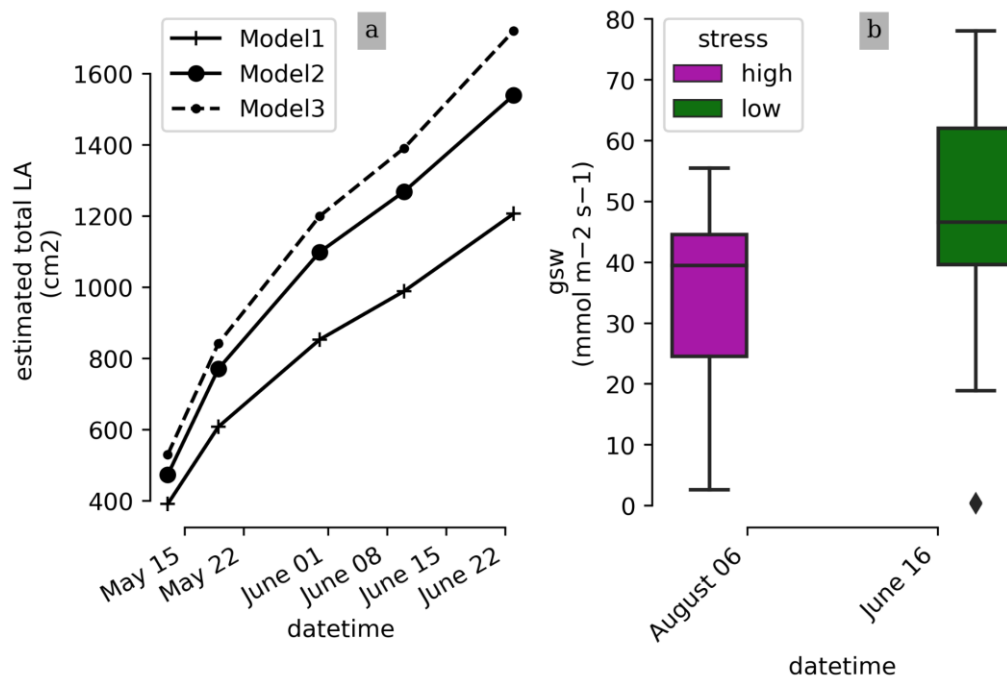
331 40, 33.6, 29.7, 28.2, 25.2, 22.4% of volumetric water content (m^3/m^3). The obtained data are fitted
332 with a least square optimization (using the Scipy library by Virtanen et al., 2020). Here we assume
333 a equal to 1 (consistent with the theoretical value), while the exponents m and n are bounded during
334 the optimization process to respectively [1.3-2.5] and [1 - 3]. With a coefficient of determination
335 R^2 of 0.97 (figure not shown), we obtained values of 1.9 and 1.2 respectively for m and n .

336 3. Results

337 3.1. Physiological response

338 Photographs of the plant at the beginning and at the end of the experiment show the increment of leaf area
339 extension of the upper part of the plant. The weekly measurements show a linear trend with time of the
340 estimated total LA (cm^2) whichever the model used (Fig. 2). At the end of the experiment water stress
341 symptoms were visible on some leaves.

342 As for the root system, the depth variations could not be precisely assessed during the course of the
343 experiment. We observed that: (i) roots reached the bottom part of the rhizotron; (ii) spread all over the
344 rhizotron with a network of primary, secondary, and root hairs without any given architecture (some roots
345 grew vertically, others in diagonals); (iii) the roots kept a white appearance with apparently no lignification
346 even for the largest roots ($\geq 3\text{mm}$).



347

348 **Figure 2: (a) Time evolution of the estimated total leaf surface area (LA) for three different model estimators. (b) leaf stomatal**
349 **conductance (High and low stress distributions are significantly different with a T-test p-value = $4.3 \cdot 10^{-3}$)**

350

351 The measurements indicate that the plant is under high water stress at the end of the irrigation cycle (one
352 week after the last partial irrigation, on June 8, 2022), and under lower water stress one day after irrigation
353 (on June 16, 2022). The mean, min, and max values of the stomatal conductance (g_{sw}) values are 37.8; 23.3;
354 55.5 $\text{mmol m}^{-2} \text{s}^{-1}$ before irrigation, respectively, and 50.6; 18.9; 78.1 $\text{mmol m}^{-2} \text{s}^{-1}$ after irrigation,
355 respectively. The result of the T-test shows that their mean values are significantly different (p-value =
356 $4.3 \cdot 10^{-3}$).

357

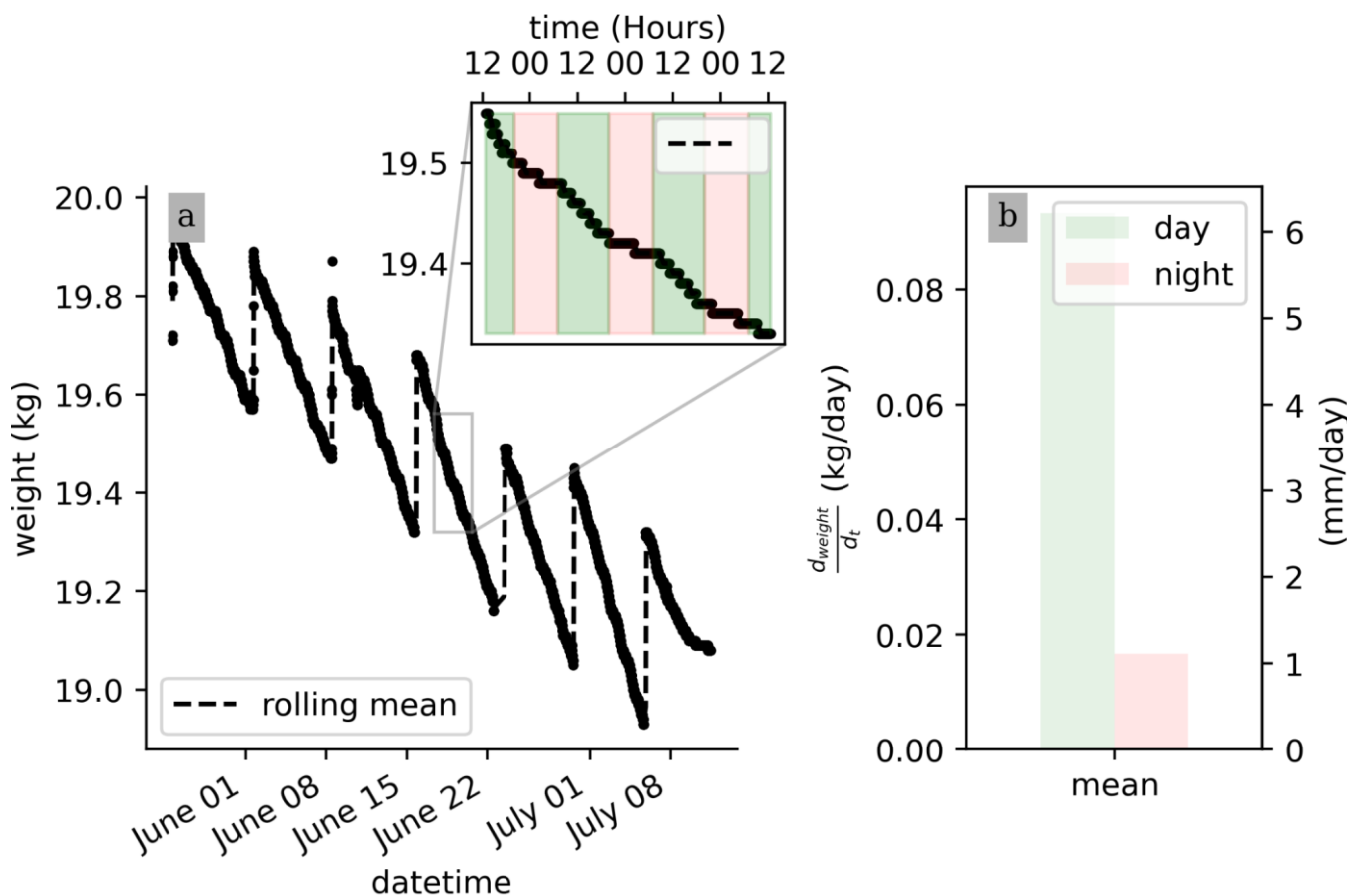
358 3.2. Transpiration rate

359 No pre-processing of the raw data is needed for their interpretation. Fig.3 shows that, on average, during a
360 PRD cycle (about one week), 0.5 kg of water transpired. Also, the weight data show that the total weight is
361 decreasing from one cycle to the next, as expected, due to the PRD protocol. Although the total water content



362 is decreasing, the transpiration rate (slope of the weight variations) remains constant for each cycle. At the
 363 very end of the experiment from July 9, an inflexion point is observed and the weight stops decreasing.
 364 Zooming on a shorter time window, the variation of the raw data weight clearly shows day/night patterns
 365 triggered by the hours when the light is switched on/off. On average, the water lost during the day is nearly
 366 20 times more than during the night (0.09 kg/day against 0.005 kg/night). Note that there is no distinction
 367 between the hours of the day (due to artificial lighting).

368
 369
 370
 371



372
 373 **Figure 3: Raw scale data collected over the course of the experiment (a) and a zoom on the week from June 20 to 25, where day and**
 374 **night periods are respectively highlighted by the green and red shaded areas. (b) Calculated daily mean transpiration (d_{weight}/dt)**
 375 **during the day (green) and night (orange) periods.**



376

377

3.3. Time-lapse ERT

378

379

380

381

382

383

384

385

386

387

388

389

390

391

392

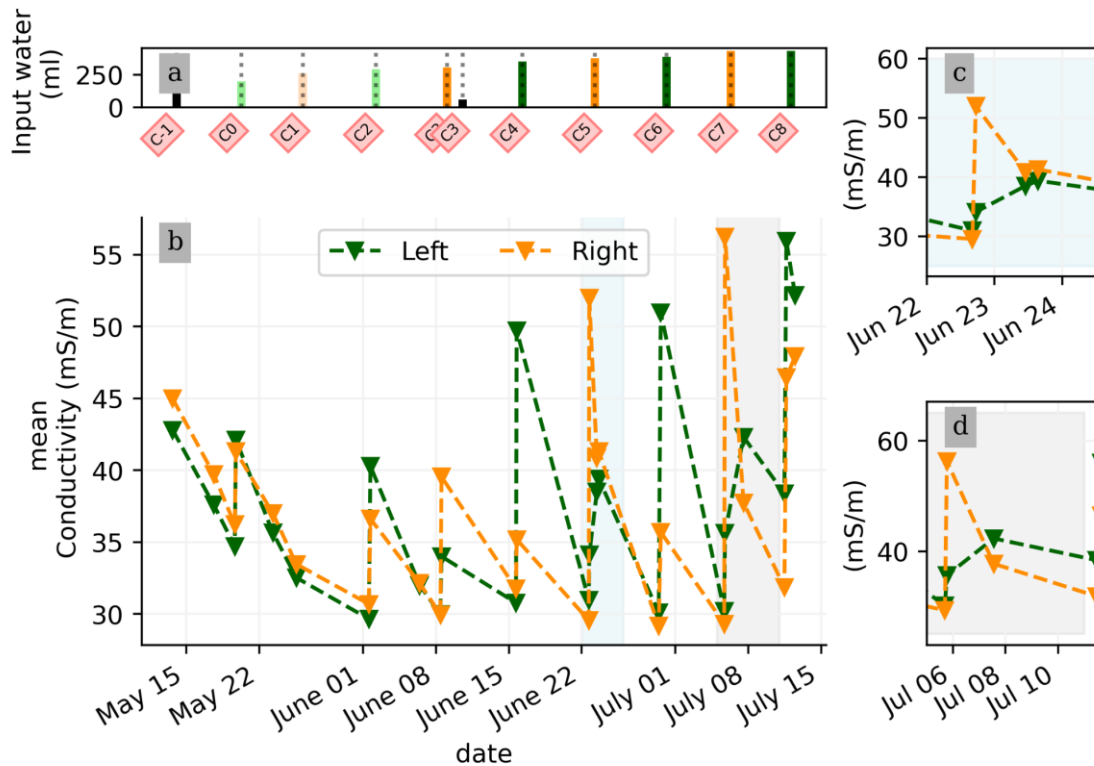
393

394

395

396

In general, the ERT data quality is very good with a small percentage of total measurements exceeding a reciprocal noise level of 5% (see Fig. A1 to A11) and with each inversion resolved within 2/3 iterations. Figure 4 shows the trend for the PRD cycles (from cycles -1 to 8) for the mean average electrical conductivity (in mS/m) for both the wet and dry sides of the rhizotron, taken as an average of each half of the ERT inversion mesh elements. When PRD is applied over only two holes (from cycle 3) the irrigated side shows a clear increase in electrical conductivity. To a much lower degree, the dry side is also affected by the water input, likely due to water redistribution during drainage. When available, the temporal dynamics between two irrigations show that the conductivity is decreasing rapidly on the irrigated side during the 2 first consecutive days and more slowly afterwards (cycles C5/6 and C7/8 respectively; Fig. 4c and Fig. 4d). As some water infiltrates also on the dry side, we also observe an increase in conductivity in it. At the end of each cycle (the cycle length is about 7 days), the rhizotron returns to the equilibrium condition, with a more homogeneous and stable average conductivity equal to 30 mS/m (mean of the dry and wet sides). This is generally true for all times, except at the end of the experiment, cycles 7 and 8, when the two sides are in different conditions.



397

398 **Figure 4:** (a) Evolution of the quantity (in ml) of water input, spatially distributed with alternating between left (green) and right
399 (orange) before and during the PRD irrigation. (b) Evolution of the mean conductivity (mS/m) average on each side, markers show
400 the acquisition time. (c) and (d) are inset zooms showing changes before and just after the irrigation event.

401

402

403

404

405

406

407

408

409

410

We selected a time window between 29 June and 5 July showing the spatial variations of the electrical resistivity before and after an irrigation event (Fig. 5). Before the irrigation, the top and lateral boundaries of the rhizotron exhibit higher ER (50 Ohm.m) than the central part (25 Ohm.m). One hour afterwards (+1H) the ER of the irrigated side had dropped by 20%.

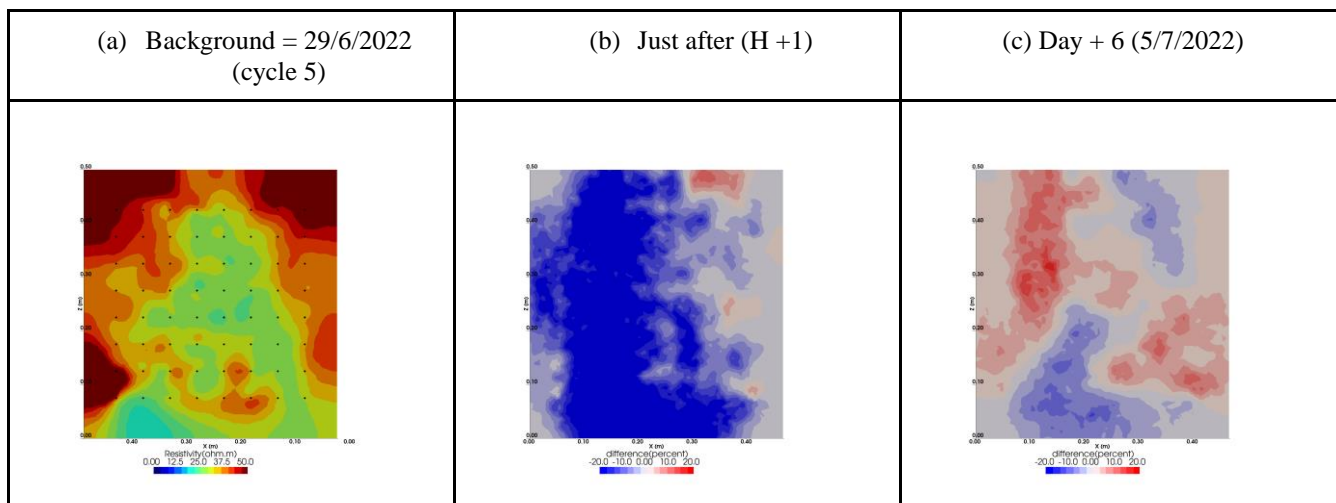
All time-lapse inversions before/after irrigation are shown in Appendix A, including before the PRD. They all show that a decrease in ER is associated with irrigation patterns while an increase in ER has a more complex spatio-temporal dynamics, not systematically associated with irrigation patterns. Changes in ER after six days (day +6) show that RWU effects are not limited to the irrigated part since the increase of resistivity was also observed on the dry part. Note from a visual inspection of the rhizotron a water table



411 forms at 0.4 m where the soil is saturated. This saturated zone level is not affected by the irrigation as no
412 increase after irrigation, and no decrease by the end of the irrigation cycles are visible. We assume that most
413 of the water fluxes were connected to the unsaturated part.

414

415



416

417 **Figure 5: Spatial distribution of the resistivity (in Ωm) and changes (in %) in electrical resistivity obtained by a time-lapse inversion**
418 **between cycles 5 and 6 following partial right irrigation of the rhizotron. Time steps correspond to measurements before (a), after**
419 **one hour (b) and after 6 days (c).**

420

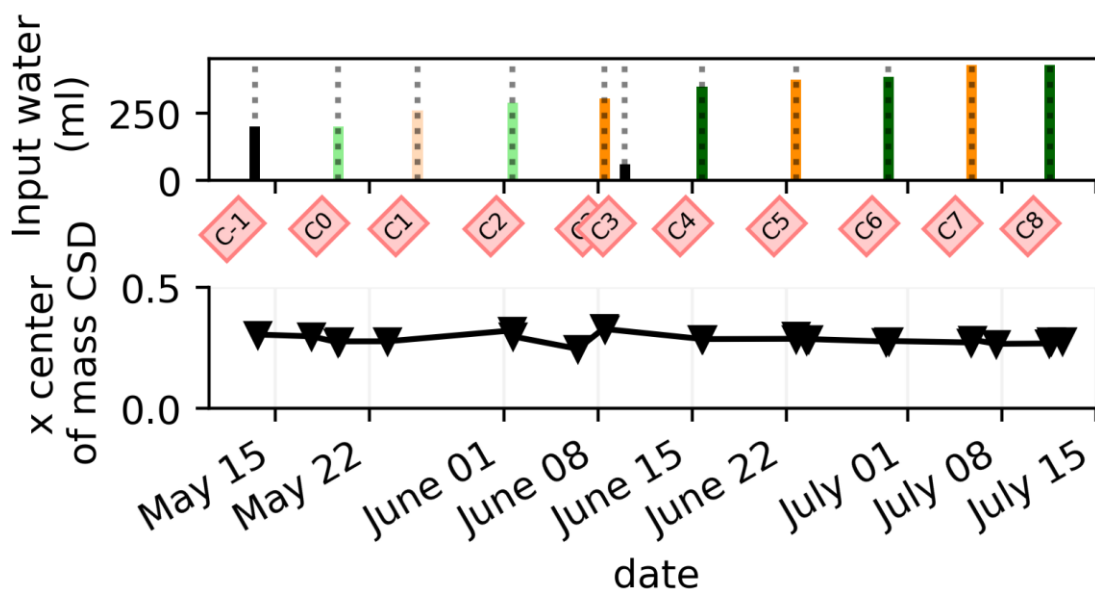
421 3.4. Time-lapse ECI

422

423 Figure 6 shows the trend of the horizontal location (x coordinate) of the centre of mass of current density
424 during the PRD cycles (from -1 to 8), after the alternative wetting events on the left and right sides of the
425 rhizotron. The soil CSD is not shown as it is always pinpointed to the location of the injection electrode
426 whatever the irrigation pattern, as expected (Figure 7abc). This result confirms the quality of the estimated
427 ER background values used for the ECI forward model. For the stem injection, the centre of mass of the
428 current source density is distributed equally from left to right except for cycle 3 when most of the current is
429 located on the left (see Fig. B1 to B4). Conversely to ER variations, the irrigation pattern does not

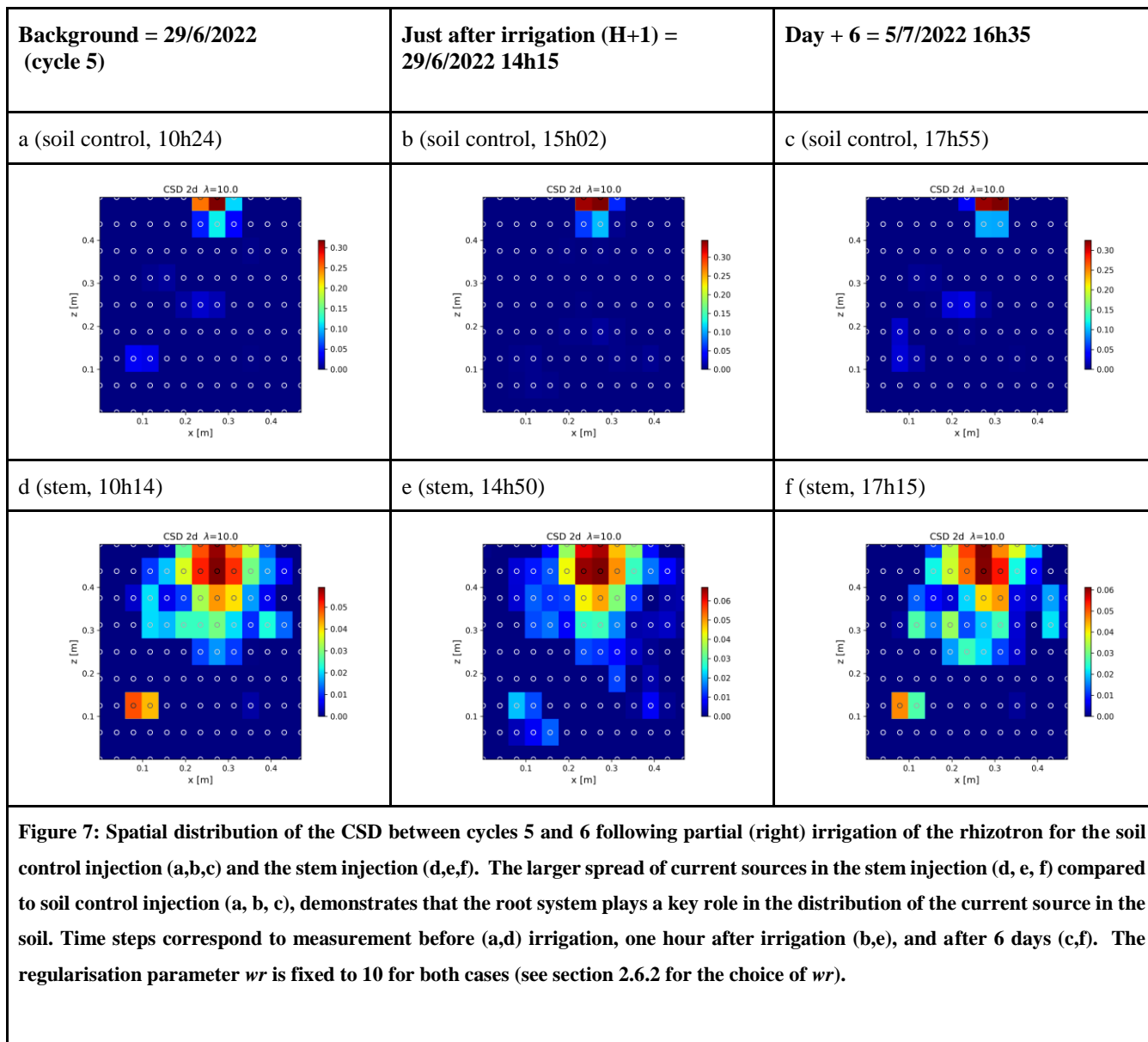


430 significantly affect the current density distribution. The same applies to the temporal dynamics between two
431 irrigations where the current density centre of mass is stable and distributed equally on both sides, as shown
432 in Fig. 7. All the time-lapse inversion results of current density for the soil and the stem injection are shown
433 in Appendix B.



434
435 **Figure 6: (a) Evolution of the quantity (in mL) of water input spatially distributed alternatively between left (green) and right**
436 **(orange) during the PRD irrigation. (b) Evolution of the centre of mass (in the x direction) of the current density, while cross markers**
437 **show the acquisition times. Cycle 5 and 6 windows were selected for the MALM time-lapse spatial analysis (Figure 7).**

438
439
440
441
442
443
444
445
446
447



448

449

450 3.5. Correlations between soil parameters and estimated transpiration rates.

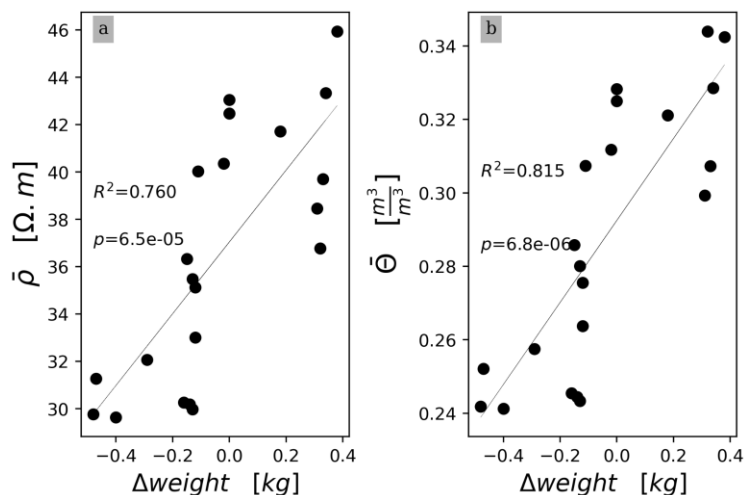
451 This section aims at drawing correlations between the soil parameters (ER, SWC, and CSD) and the
 452 transpiration estimated from the rhizotron weight data. We do not account for the weight variations due to
 453 the plant and root growth material (as this can be considered negligible relative to water dynamics).



454 Figure 8 shows the relationship between the variation between two consecutive measurements of the weights
455 with the variations of average electrical resistivity (Fig.8a, $R^2=0.76$, $p\text{-value}=6.5 \times 10^{-5}$) and those of
456 resistivity-derived average water content (from Archie's law - Fig.8b, $R^2=0.815$, $p\text{-value}=6.8 \times 10^{-6}$). An
457 increase in weight over time is positively correlated with an increase in in resistivity and water content
458 meaning that the changes in resistivity are mainly associated with transpiration (rather than changes in soil
459 structure or other parameters).

460 For each node of the mesh, ER values are translated to SWC using Archie's law with the calibrated
461 parameters m and n (see Sect. 2.6.3). To simplify, we assume that both porosity and fluid water conductivity
462 are homogeneous in space and time (i.e no mixing between the tap water used for cycle 3 and the nutrient
463 solution for all the other times). The maximum SWC observed after irrigation is about $0.42 \text{ m}^3/\text{m}^3$ (figure
464 not shown). The minimum SWC of about $0.25 \text{ m}^3/\text{m}^3$ is repeatedly observed (see Fig. C1) just before each
465 irrigation, meaning that the driest times are below field capacity conditions (estimated at $0.4 \text{ m}^3/\text{m}^3$).
466 Translated ER to SWC improve slightly the strength of the correlation with the transpiration (variations of
467 weight) due the non-linear nature of Archie's law.

468
469
470



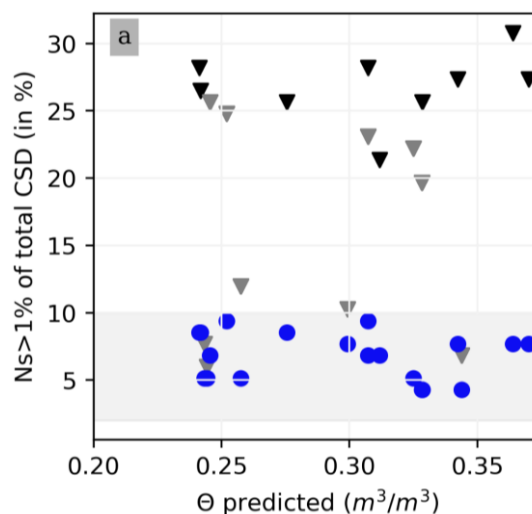
471



472 **Figure 8: Relationship between time variation of weight and the time variation of the average electrical resistivity (a) and of the**
473 **average estimated water content (b) in the rhizotron. Straight lines show the linear regression fit obtained. All cycles are**
474 **considered.**
475

476

477 Figure 9 shows the relationship between the variation of the percentage of the current sources carrying at
478 least 1% of the total density (N_{s1}) used as an estimator for current density dispersion with respect to the
479 SWC. For the soil injection (blue dots), N_{s1} is relatively constant between 5 to 10% of the total number of
480 possible injection nodes (grey area) irrespective of the SWC values (spanning the whole range of volumetric
481 water content from 0.25 to 0.42). For the stem injections, we distinguish between values after (black
482 triangles) and before (grey triangles) cycle 3, for which no stress has been applied (grey triangle Fig. 9). For
483 the stem injection, for cycles where stressed was applied, N_{s1} is 4 to 5 times (appr. 25 to 30% of the sources
484 carrying at least 1% of the total current density) more than for the soil. For cycles where stressed was not
485 applied (i.e. < cycle 3), for the stem injection, N_{s1} is distributed between 5 and 25%. No trend between the
486 current spread with increasing water content levels is visible. From Figure 9, we noticed that the current
487 spreads less before the actual PRD (grey triangles) started than after (black triangles).



488

489 **Figure 9: (a) Relationship between the number of the current sources (N_s) carrying at least 1% of the total density ($A \cdot m^{-2}$) with**
490 **respect to the estimated SWC (m^3/m^3). CSD results are obtained after inversion with a regularisation parameter w_r of 10. Cases of**
491 **the stem before cycle 3 (grey), after cycle 3 (black) and the soil (blue) injections. All cycles are considered.**



492

493 4. Discussion

494 4.1. Validity of ERT and ECI in demonstrating the effects of the PRD irrigation scheme

495 Our first assumption was that the variations in ER (or in SWC inferred from the ER) are relevant as a proxy
496 of root activity. Its validity has been checked against direct observation using the variations of weights
497 measured from the scale data used as an indicator of plant transpiration. On average, in our experiment, the
498 plant maintained high rates of transpiration to about 6 mm/day for each cycle except for the last cycle
499 (number 9) where a decline was observed (Fig. 3). This range is in line with another rhizotron experiment
500 where narrow-leaf lupin plants were grown: Garrigues et al. (2006) measured a mean rate of 3 mm/day. It is
501 commonly found in the scientific literature that changes in ER are associated with root activity (e.g., Michot
502 et al.,2003; Garré et al.,2011; Cassiani et al., 2015; Whalley et al., 2017). Here we had further confirmation
503 of this, with a significant correlation between ER changes and gravimetric soil moisture changes (derived
504 from the load cell) (Fig. 8). The leaf stomatal conductance and visual observation of plant above- and below-
505 ground material growth were additional ancillary data to interpret the general state of the plant. Our
506 observation is in line with the literature i.e. in general, low soil water content (SWC) can lead to drought
507 stress in plants, which can result in decreased leaf stomatal conductance and less transpiration, and vice-
508 versa.

509
510 A second assumption was that, when applying the PRD, only one part of the root system would be active
511 and the current injected in the stem would only spread to the side where the root system is irrigated. This
512 assumption was not directly supported by the observations. Figures 6 and 7 show that the influence of the
513 irrigation pattern was negligible on the spatial distribution of the inverted CSD and that the current
514 distribution was not correlated with ER variations. It is true that active roots have higher hydraulic
515 conductivity but on the other hand, increased membrane permeability may encourages current leakage into
516 the soil. We nevertheless noticed that the CSD spatial distribution, while the rhizotron is irrigated at its full



517 length (cycles -1 to 2), was significantly different from the side irrigation cycles (Fig. B4). Indeed,
518 homogeneous irrigation without applying stress to the plant results in a very shallow current leakage. This
519 is a hint that the hydraulically stressed plant tends to have a wider and deeper active root system, even not
520 necessarily active only on the side where the PRD is temporarily applied. Possibly the reaction of the plant
521 to the changing side is too slow to show up in our measurements, but the reaction to general stress is apparent.
522

523 **4.2. Effect of soil water content**

524 Soil water content can affect the distribution of the current leakage by influencing the minimum resistance
525 pathways, i.e., whether roots and/or soil provide the minimum resistance to the current flow. Literature
526 reports that electrical capacitance method better estimates crop root traits under dry conditions (Gu et al.,
527 2021). In order to make a comparison with capacitance studies, we assumed that if the current distribution
528 remains unchanged (i.e. leaking into the same areas), there must be minimal changes in the electrical
529 capacitance. In this study, supposing no impact of the initial model, Fig. 9 shows that there is no apparent
530 effect of the soil water content on the current density distribution. Note that the soil water content estimated
531 is the bulk contribution of roots and soil, as only one pedophysical relationship was used, while recent studies
532 tend to show that mixed soil-root pedophysical relationships are preferable (e.g. Rao et al., 2018). This is
533 clearly limiting our ability to interpret the independent contribution of the soil and the roots, yet this does
534 not limit our ability to identify zones where water availability leads to root water uptake.

535 **4.3. Possible mitigation of the PRD effect**

536 In general, a PRD irrigation experiment must comply with two criteria: (1) a minimum soil water content to
537 trigger a physiological response and, (2) a distinction between a wet and a dry side (Stoll, 2000). While the
538 first criterion complied in our experiment, the second did not. And the latter is a very interesting piece of
539 evidence. The following considerations apply.



- 540 (1) According to McAdam et al. (2016) and Collins et al. (2009), ABA is triggered even by mild soil
541 stress values. Consequently, plants adapt the hydraulic conductivity of their roots as well as that of
542 the soil in their vicinity through exudates (Carminati and Javaux, 2020). Results from previous
543 irrigation experiments using PRD have shown that changes in stomatal conductance and shoot
544 growth are some of the major components affected (Düring et al., 1996). In our experiment, the
545 shoot growth fitted with the conventional leaf area and growth models, except at the end of the
546 experiment when signs of water stress were visible on some leaves. The magnitude of the shoot
547 growth is correlated with the number of roots. Drought may cause more inhibition of shoot growth
548 than of root growth (Sharp and Davies, 1989). Although the root system was already well developed
549 it is not possible to exclude its development as a factor influencing the CSD distribution.
- 550 (2) The spatiotemporal analysis of the ER showed that the water changes were not limited to root
551 effects. Water redistribution from dry to wet in the soil and from shoot to dry roots (Smart et al.,
552 2005, Lovisolo et al., 2016) may have occurred (Fig. A1 to A11). Additionally, capillary rise may
553 have taken place due to the presence of a saturated zone at the bottom of the rhizotron. Due to the
554 fact that water drained on both sides, RWU was not only vertically distributed but also horizontally.
555 The range of water content varied significantly with a minimum SWC of about $0.25 \text{ m}^3/\text{m}^3$,
556 repeatedly observed just before each irrigation meaning that the driest times are below field capacity
557 conditions (estimated at $0.4 \text{ m}^3/\text{m}^3$). Drying half of the root system resulted in a reduction of the
558 stomatal conductance (based on the mean of the distribution) of the order $5 \text{ mmol m}^{-2} \text{ s}^{-1}$ after a 1
559 week cycle. Given the stress applied, the ER changes highlighted that root played a major role in
560 the wine plant survival and evidenced strategies of adaptation. Indeed, the plant was able to change
561 its water uptake zones depending on the water availability, from all places, not only from the
562 alternate irrigated areas.
- 563 (3) Finally, in order to know if the PRD conditions are met it would have been important not to neglect
564 the different states of root growth, and root renewal (because of renewal and decay) with respect to



565 the geophysical data. Nevertheless, this would have required opening and scanning the rhizotron
566 with conventional methods. Finally, we did not make a distinction between the hours of the day
567 although the changes observed for the irrigation are rapid, usually at the hourly scale, and could be
568 similar for RWU.

569

570 **4.4. Performance of the acquisition protocol and the processing**

571

572 We discuss here how the quality of the recovered current density models by evaluating the performance of
573 the protocol and the processing. First, it is important to note that although the ERT data quality was really
574 good (very few reciprocals were rejected, see Table A1), the inverted model was not perfect and this
575 ultimately has an impact also on the ECI forward model. The algorithm has been tested already in a rhizotron
576 experiment and is capable of distinguishing between punctual sources with the lowest current carried of 5%
577 of the total current (Peruzzo et al., 2020). The CSD resolution, of course, matches the electrode interspace
578 (in this case 5cm) and the smoothness constraint does not impact the simulation of point source
579 reconstruction. We adopted an inversion without any prior information to recover the current density. Only
580 model smoothing was applied by weighting the model data by an optimal factor of 10 inferred from an L-
581 curve analysis. Similar to the ERT inversion, the ICSD the problem is also ill-posed. In this case, the 4-
582 electrodes setup ensures that the current will flow through the plant after injection, regardless of the contact
583 resistance. However, the accuracy of the measured data may be impacted by contact resistance, as errors in
584 the measured resistance will negatively affect the quality of ERT and ICSD inversions. The impact is more
585 pronounced on ICSD, as it is dependent on ERT. Lastly, because the box is relatively small and no-current-
586 flow boundary conditions (Neumann) are imposed, we may expect an effect due to the position of the return
587 electrode where the current is attracted due to the strongest gradient nearby (Mary et al., 2019b).

588

589



590 4.5. Outlook

591 In order to strictly correlate PRD effects with geophysical measurements, one should consider a physical
592 barrier to separate the two sides of the rhizotron to a split-roots configuration. Another option is to increase
593 the lateral size to prevent redistribution or to use a very percolating material such as glass beads, gravels or
594 coarse sands. This should be carefully considered, as the rhizotron must also be an environment where plant
595 growth is possible under “natural” conditions, and for this some water retention capacity is needed for the
596 soil. A larger drainage capacity would simplify the interpretation as no-water redistribution from one side to
597 the other can occur. Although considering a barrier is technically possible, it would require a more complex
598 inversion scheme of the ERT and ECI considering that no electrical current can flow from side to side. One
599 could also consider increasing the measurement frequency to catch processes at an hourly scale and
600 comparing day/night measurements, particularly those associated with water redistribution from the stem
601 back to the roots at night when transpiration is reduced and its effect on the water status of the roots. As we
602 have seen that most of the water changes occurred in the day consecutive to the irrigation, catching rapid
603 changes of ER would help drive a conclusion on how much ECI is connected to the active root zone. Finally,
604 in order to draw robust statistical conclusions, the experiments should be replicated for multiple plant
605 samples.

606 5. Conclusion

607 The study aimed at understanding the current path in the root system and active root zones using geoelectrical imaging,
608 considering soil water content and irrigation regimes. Electrical Resistivity Tomography (ERT) is sensitive to both irrigation
609 and RWU processes. The ECI model uses a physical approach to measure current density after stem stimulation. The CSD was
610 very different from the control soil injection to the stem injection but nevertheless did not correlate with PRD cycles as
611 originally expected. We demonstrate that under mild stress conditions, it is practically impossible to spatially distinguish the
612 PRD effects using the ECI. We only evidenced that the Current Source leakage depth varied during the course of the experiment
613 but without any significant relationship to the Soil Water Content changes or evaporative demand. A few aspects of the

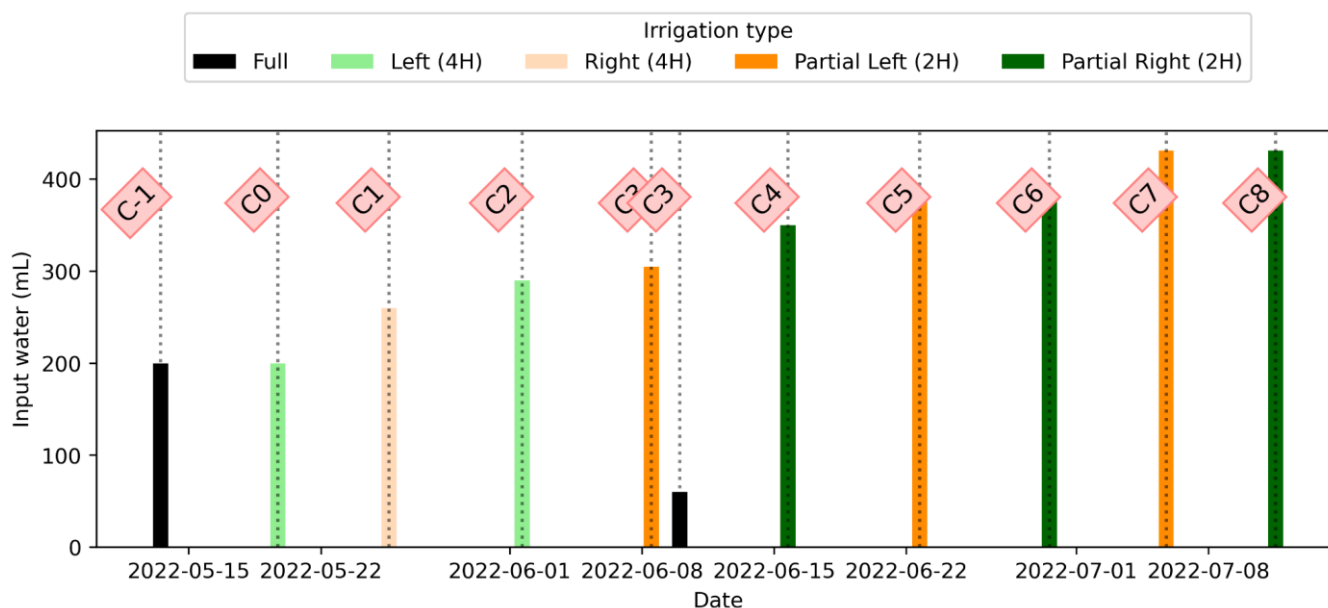


614 experiment would gain to be more closely studied such as the water redistribution that possibly also affects current distribution.
 615 In the future, we expect to improve our understanding by coupling the geophysical experiment with an unsaturated soil-plant-
 616 atmosphere model.

617 6. Appendices

618 Appendix A: Time-lapse ERT inversion results

619 As we selected only one cycle in the manuscript, we report here further details about the time-lapse ERT inversion results for
 620 all the cycles. The inversion procedure is equivalent to the one described in Sect. 2.6.1 of the manuscript (Data processing -
 621 Analysis of the ERT data). All time-lapse inversion models are plotted with a unique scale ranging from -20 to 20% of changes.
 622



623
 624 **Figure A1: Evolution of the quantity (in mL) of water input spatially distributed with an alternate between left (green) and right**
 625 **(orange) during the PRD irrigation. The black bars hold for full-width irrigation (over all the holes, see fig. 1 manuscript), light**
 626 **green and orange bars hold for irrigation over the 4 sides of holes, and dark green/orange for 2 holes irrigation.**

627
 628
 629

Background = 13/5/2022 16h25 (cycle -1)	Day + 4: 17/05/2022 15h00 (cycle -1)	Day + 6: 19/5/2022 15h38 (cycle -1)
--	---	--

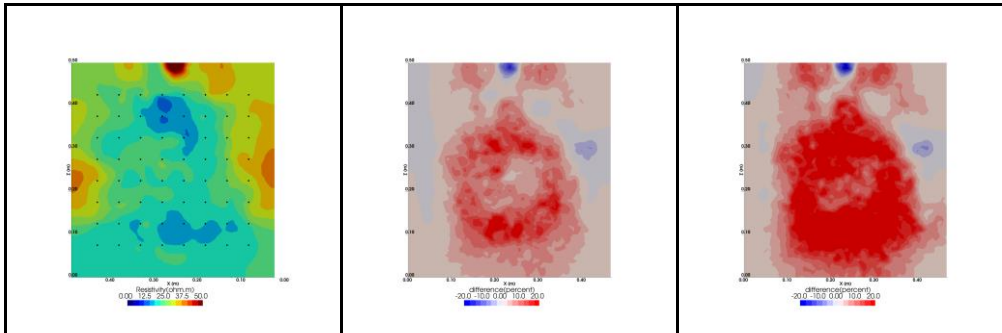


Figure A2: Cycle -1 (2022-05-13 through all the upper holes)

630

631

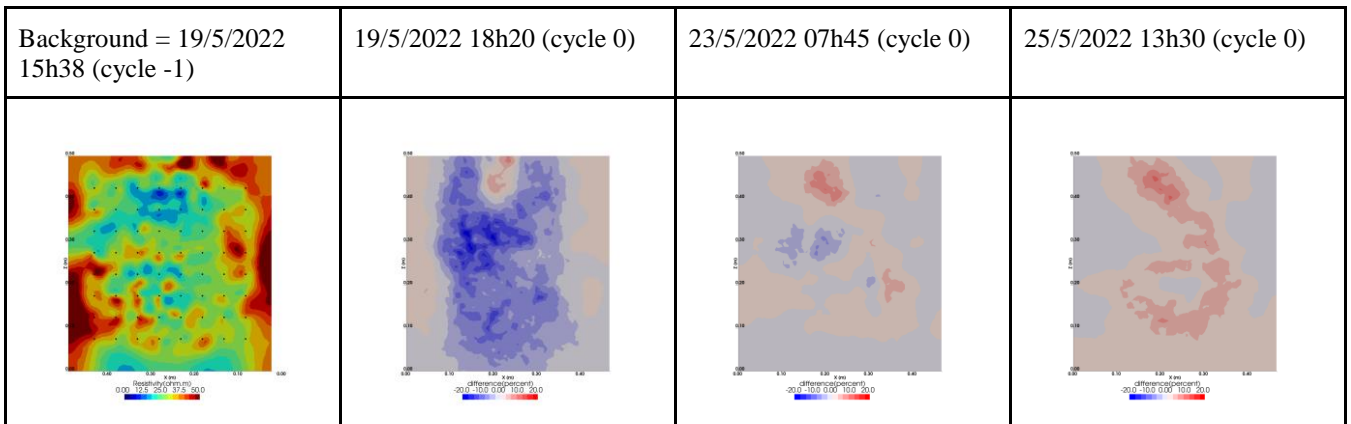


Figure A3: Cycle -1 to 0 (partial irrigation: 19/05/2022 17:00-17:30 200 ml through the first 4 upper holes (left side), no outflow through 72)

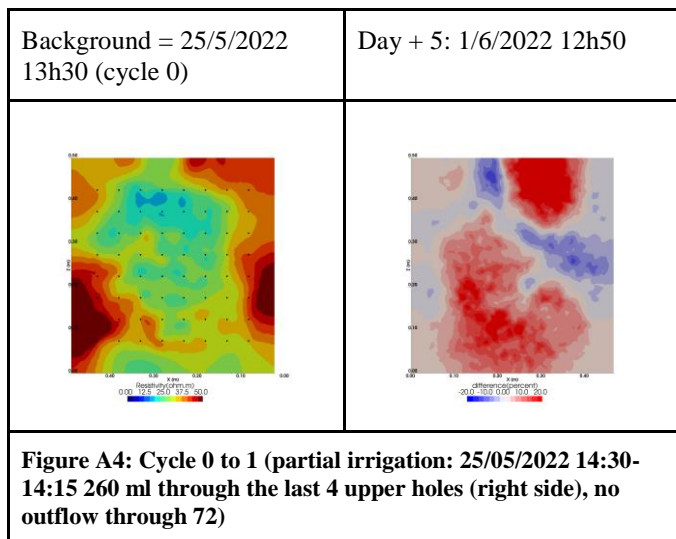
632

633



634

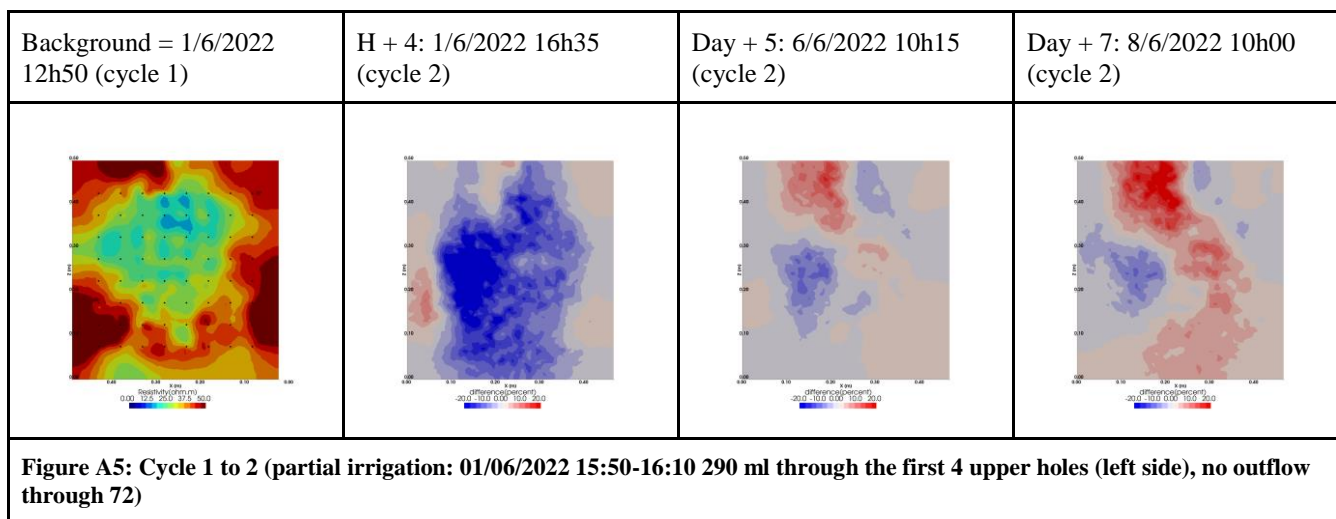
635



636

637

638



639

640

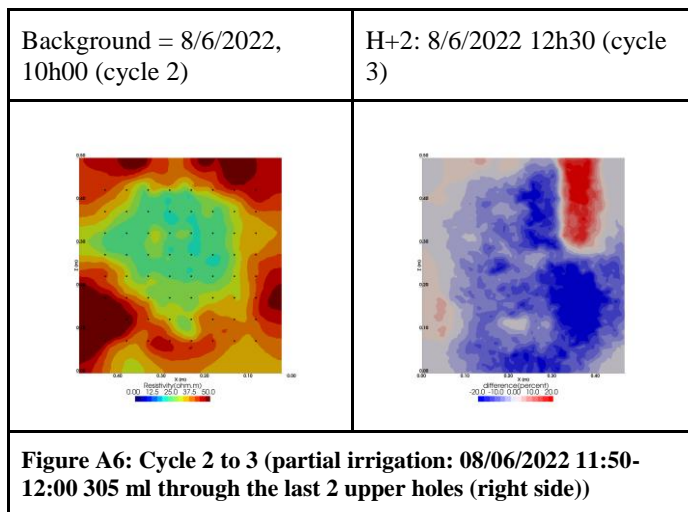
641

642

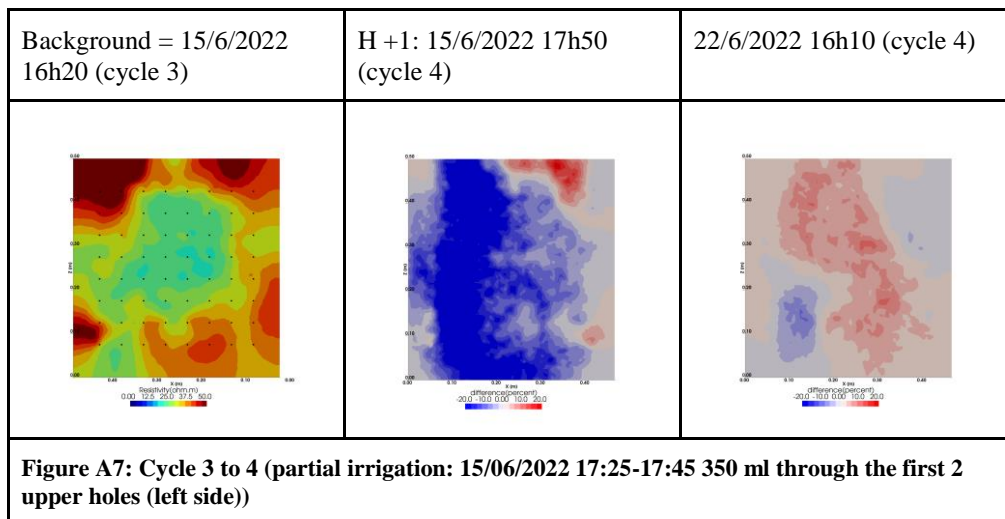
643

644

645



646



647

648

649

650

651

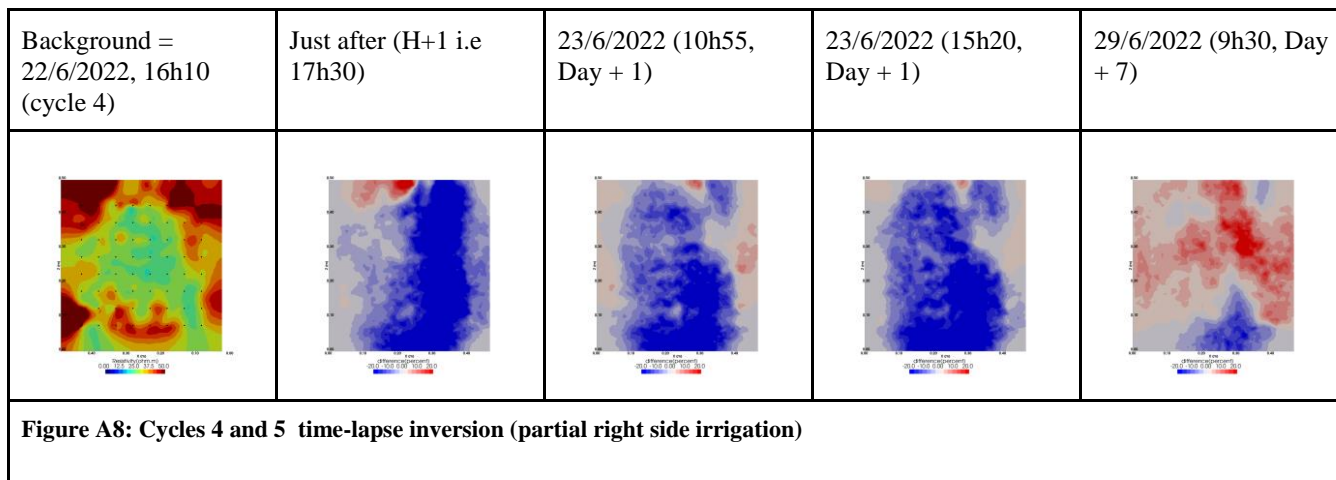
652

653

654

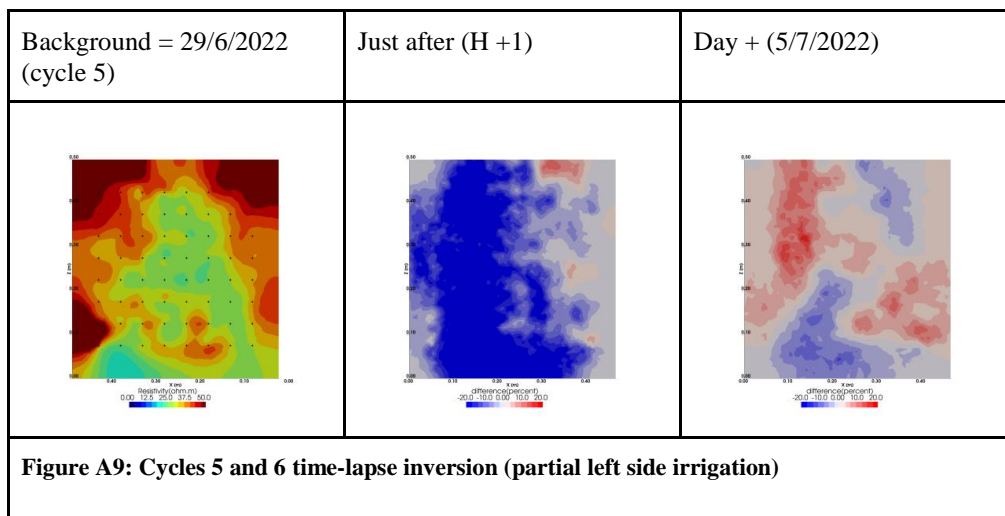
655

656



657

658



659

660

661

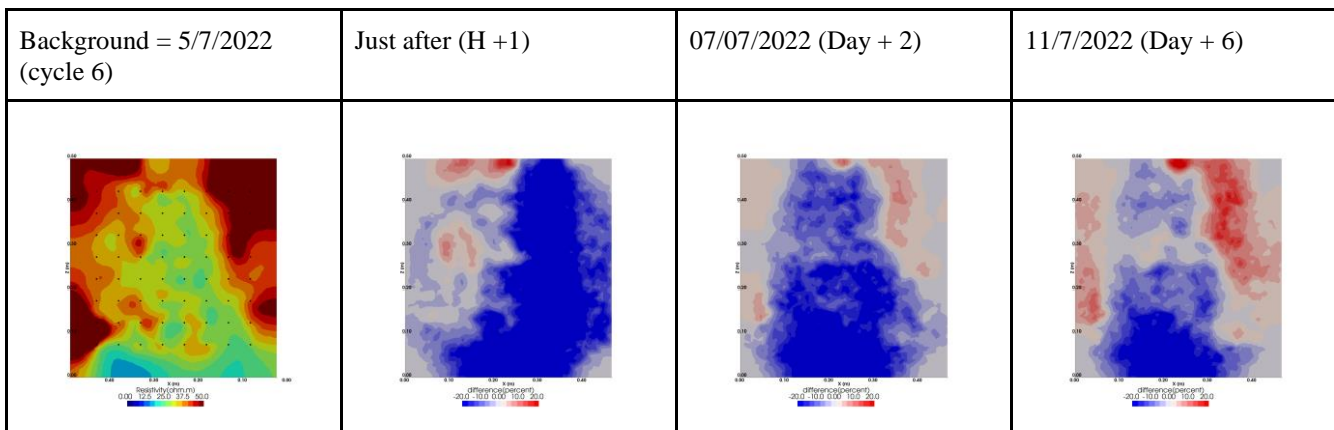


Figure A10: Cycles 6 and 7 time-lapse inversion (partial right side irrigation)

662
 663
 664

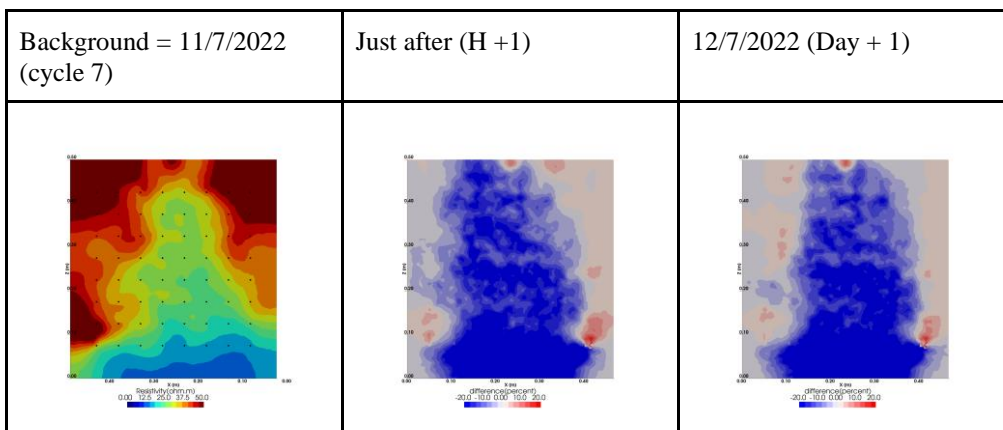


Figure A11: Cycles 7 and 8 time-lapse inversion (partial right side irrigation)

665
 666
 667
 668
 669
 670
 671
 672
 673



Date	RMS (%)	# measurements read (over 2484)
2022-06-01 12:50:00	1.36	2048
2022-06-01 16:35:00	1.15	1920
2022-06-06 10:15:00	1.53	2268
2022-06-08 10:00:00	1.41	2230
2022-06-08 12:30:00	1.16	2028
2022-06-15 16:20:00	1.08	2137
2022-06-15 17:50:00	1.47	1493
2022-06-22 16:10:00	1.38	2109
2022-06-22 17:21:00	1.14	1372
2022-06-23 10:55:00	1.48	2229
2022-06-23 15:20:00	1.38	2268
2022-06-29 09:30:00	1.27	2075
2022-06-29 14:15:00	2.04	2027
2022-07-05 16:35:00	1.7	2067
2022-07-05 18:25:00	1.85	980
2022-07-07 13:15:00	1.98	2225
2022-07-11 11:20:00	2.5	2093
2022-07-11 15:50:00	2.72	2238
2022-07-12 12:00:00	2.68	2255

674 **Table A1: Table summarising the final RMS and the number of data used for each individual inversion**

675

676

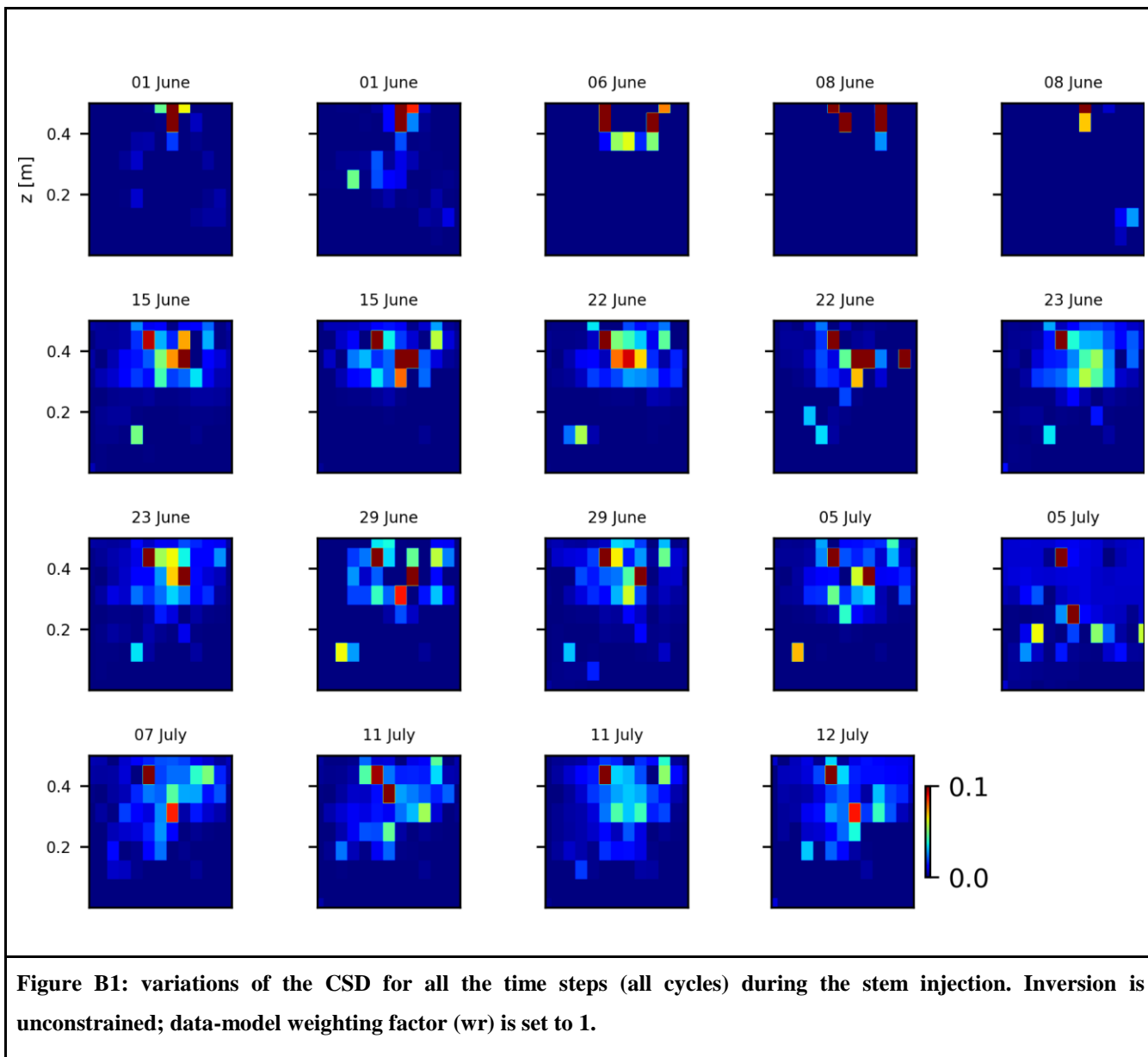
677



678 **Appendix B: Inversion of current density (ICSD)**

679

680 As we selected only one cycle in the manuscript, we report here further details about the time-lapse ICSD inversion results for
681 all the cycles. The inversion procedure is equivalent to the one described in Sect. 2.6.2 of the manuscript (Data processing -
682 Analysis of current density) and we invite the reader to refer to Peruzzo et al. (2020) for a full description of the algorithm.
683 Furthermore, we extend the analysis showing the effect of the model regularisation (smoothing). Figures B1 and B2 show the
684 current density evolution with the time respectively for the stem and the soil injection with a regularisation parameter of 1.
685 The same is for Figures B3 and B4 with a regularisation of 10.



686

687

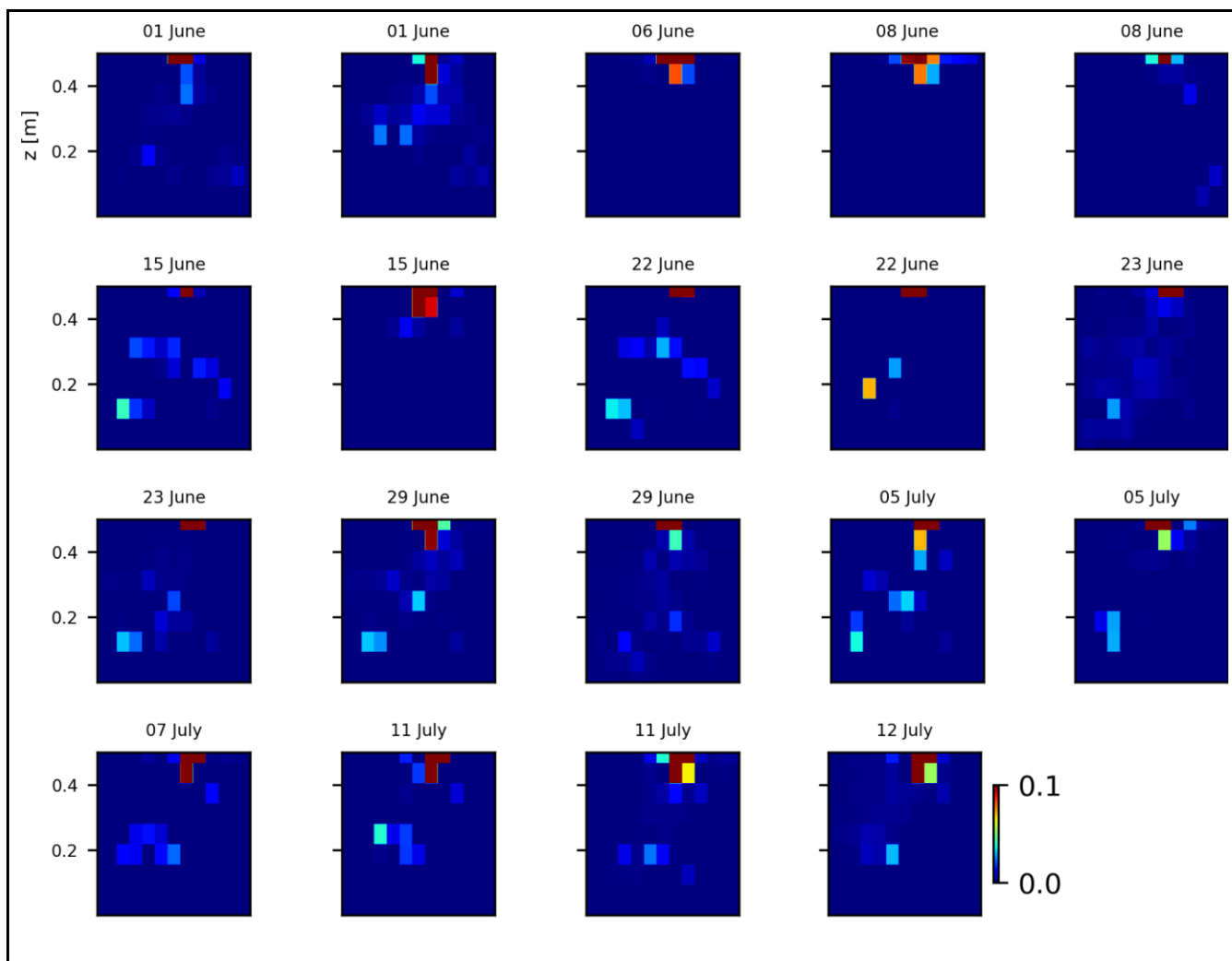


Figure B2: variations of the CSD for all the time steps (all cycles) during the soil control injection. Inversion is unconstrained; data-model weighting factor (w_r) is set to 1.

688
689
690
691
692

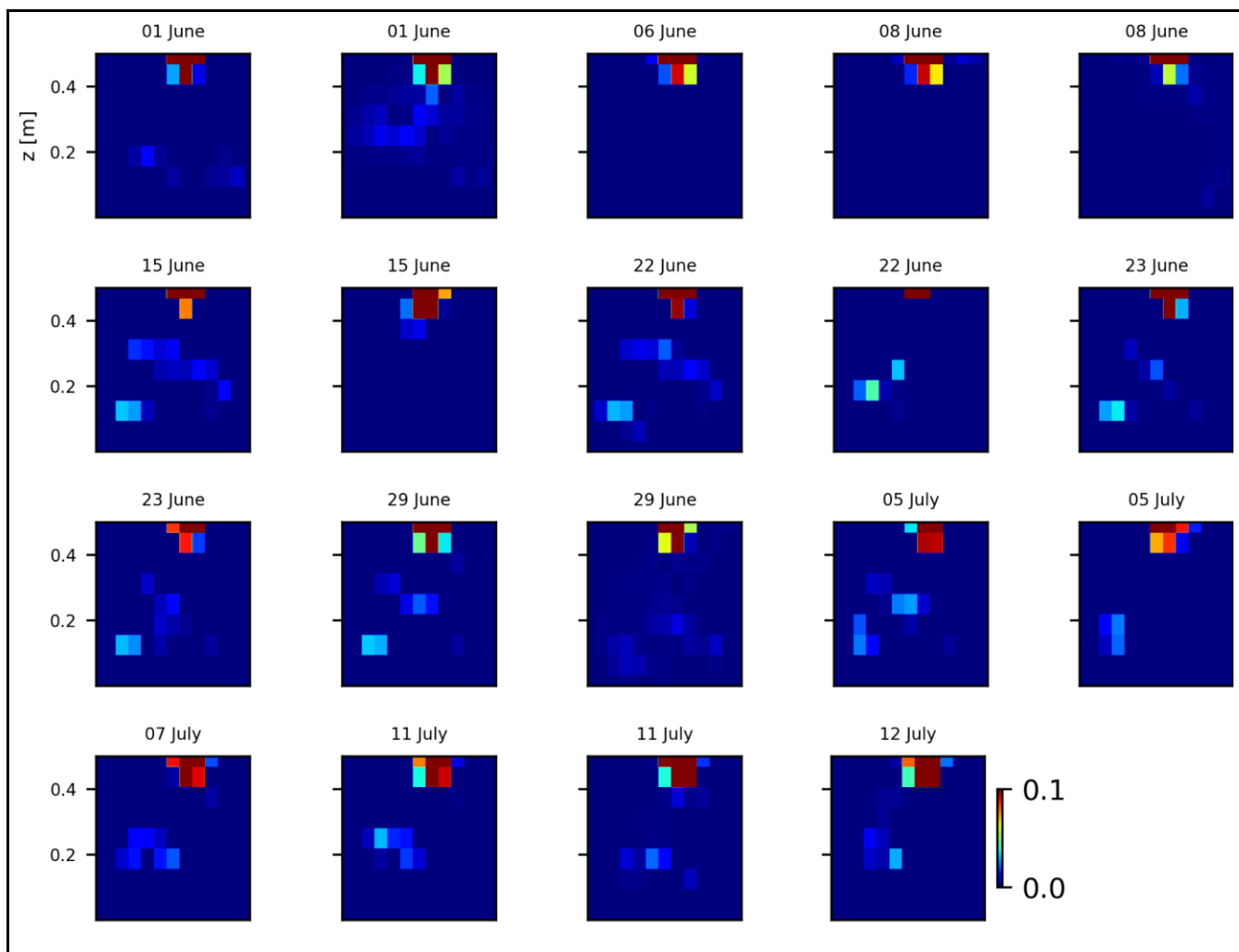


Figure B3: variations of the CSD for all the time steps (all cycles) during the soil control injection. Inversion is unconstrained; data-model weighting factor (w_r) is set to 10.

693
694

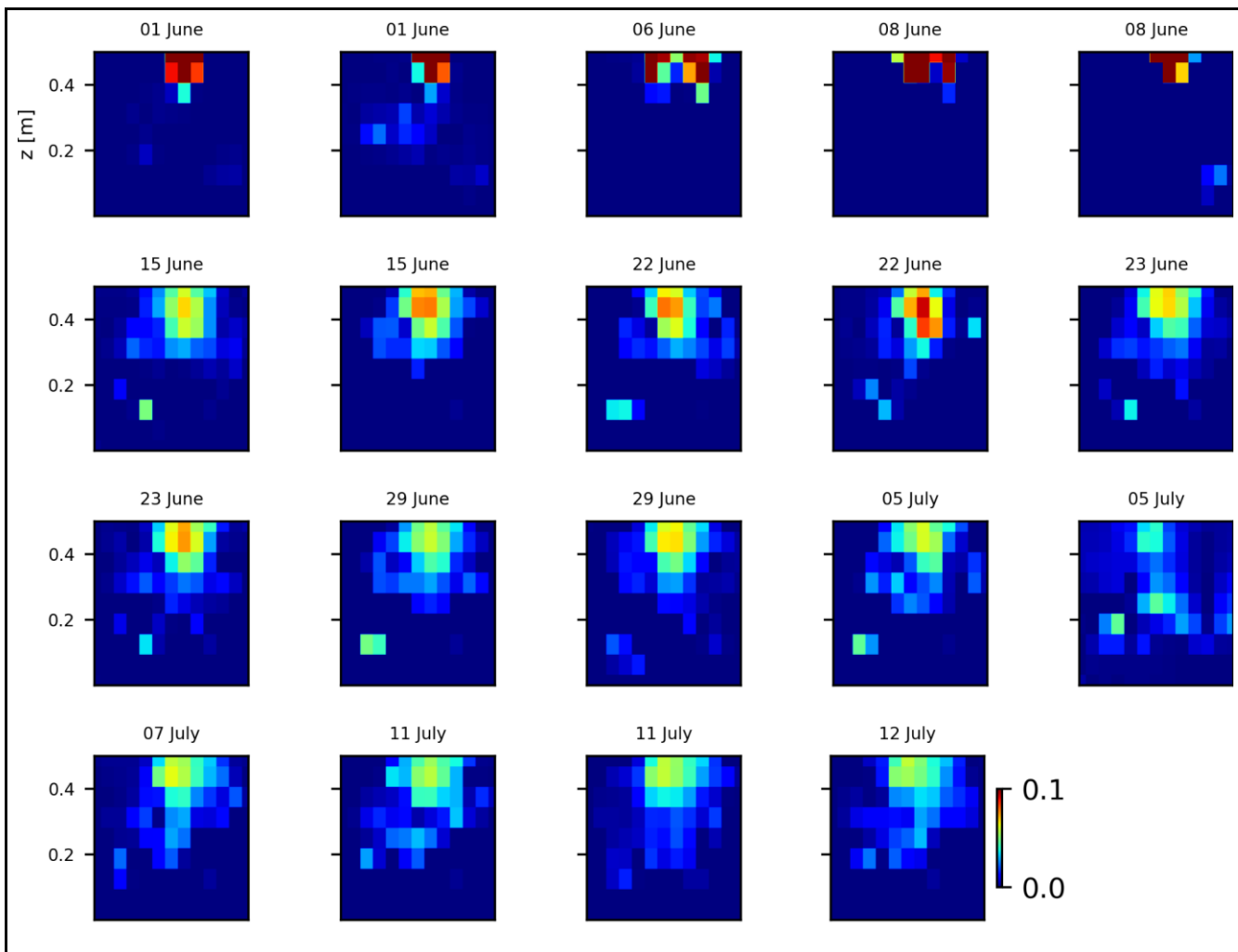


Figure B4: variations of the CSD for all the time steps (all cycles) during the stem injection. Inversion is unconstrained; data-model weighting factor (w_r) is set to 10.

695
696
697
698

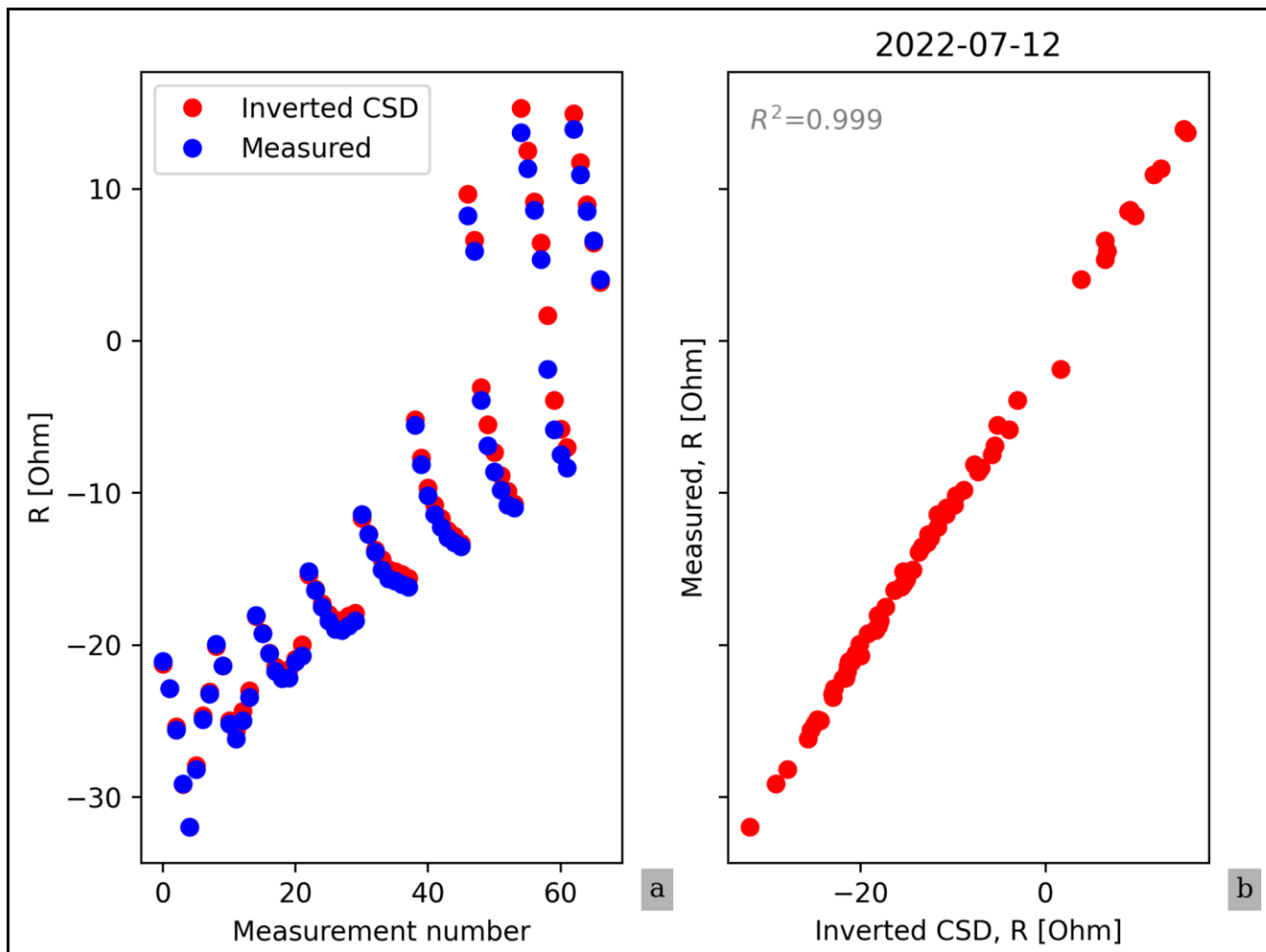


Figure B5: Evaluation of the quality of the CSD inversion for the acquisition date 2022-07-11. The linear correlation coefficient is always > 0.95 for all the time steps.

699

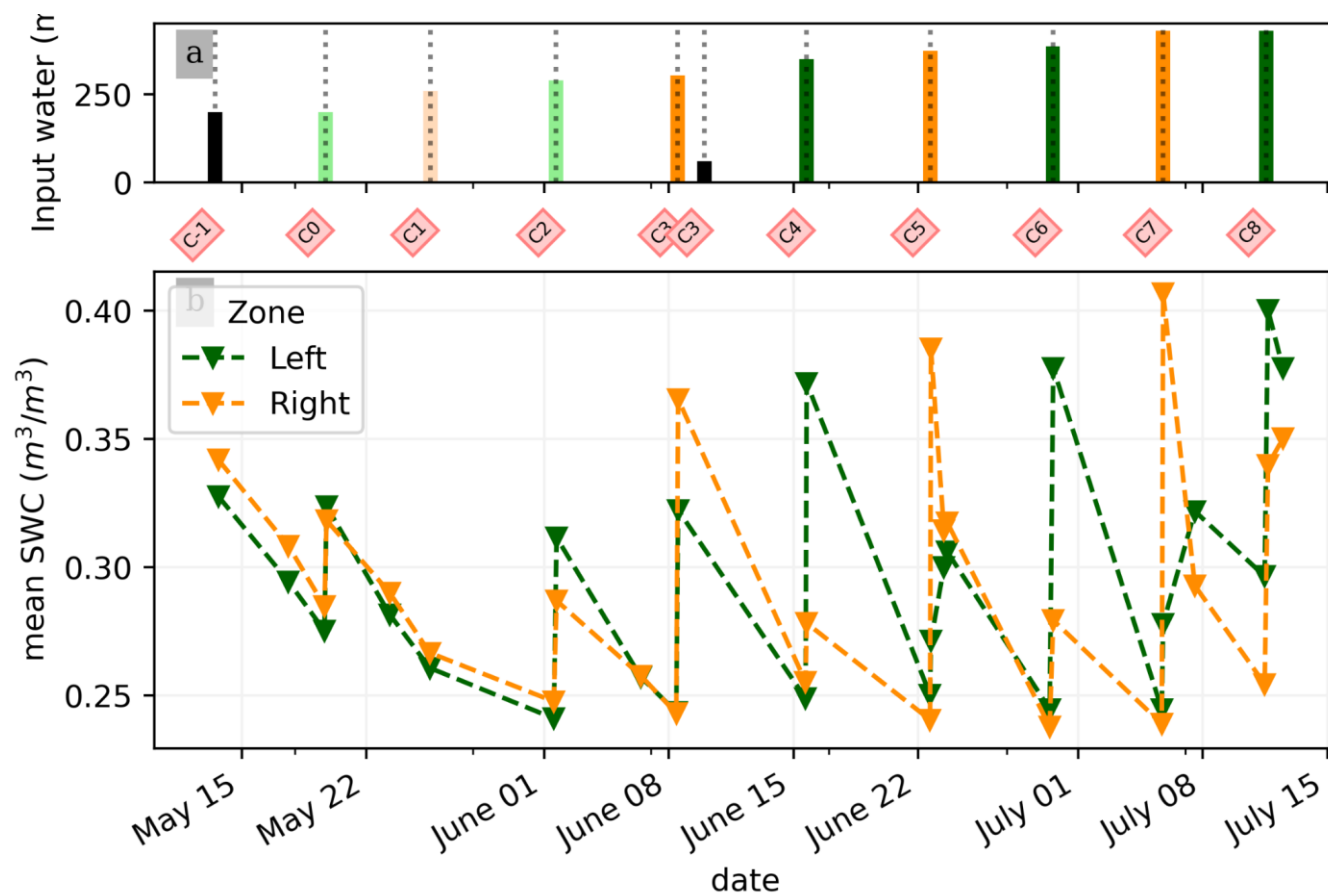
700



701

702 **Appendix C: Soil Water Content converted variations**

703



704

705 **Figure C1: (a) Evolution of the quantity (in mL) of water input spatially distributed with an alternate between left**
706 **(green) and right (orange) during the PRD irrigation. The black bars hold for full-width irrigation (over all the holes,**
707 **see fig. 1 manuscript), light green and orange bars hold for irrigation over the 4 sides of holes, and dark green/orange**
708 **for 2 holes irrigation. (b) Evolution of the mean SWC (m³/m³) average on each side, markers show the acquisition**
709 **time.**

710 **7. Data availability**

711 Codes and data to reproduce figures articles are available in the Zenodo data repository (link to come after decision).



712

713

714 *Competing interests*

715 The authors declare that they have no conflict of interest.

716

717 *Author contribution*

718 BM, VI, LP, FM, BR, CC, YW and GB designed the experiments, and BM, VI, BR and FM carried them out. BM, LP, GB ,
719 CC developed the model code and performed the simulations. BM prepared the manuscript with contributions from all co-
720 authors for writing – review & editing.

721

722

723 *Acknowledgments*

724 Benjamin Mary acknowledges the financial support from European Union’s Horizon 2020 research and innovation programme
725 under a Marie Skłodowska-Curie grant agreement (grant no. 842922).

726

727 **References**

728 1. Archie, G. E.: The Electrical Resistivity Log as an Aid in Determining Some Reservoir Characteristics, Trans. AIME,
729 146, 54–62, <https://doi.org/10.2118/942054-G>, 1942.

730 2. Binley, A.: 11.08 - Tools and Techniques: Electrical Methods, in: Treatise on Geophysics (Second Edition), edited
731 by: Schubert, G., Elsevier, Oxford, 233–259, <https://doi.org/10.1016/B978-0-444-53802-4.00192-5>, 2015.

732 3. Binley, A. and Slater, L.: Resistivity and induced polarization: theory and applications to the near-surface earth,
733 Cambridge University Press, Cambridge, UK ; New York, NY, 2020.

734 4. Blanchy, G., Saneiyani, S., Boyd, J., McLachlan, P., and Binley, A.: ResIPy, an intuitive open source software for
735 complex geoelectrical inversion/modeling, Comput. Geosci., 137, 104423,
736 <https://doi.org/10.1016/j.cageo.2020.104423>, 2020.

737 5. Carminati, A. and Javaux, M.: Soil Rather Than Xylem Vulnerability Controls Stomatal Response to Drought, Trends
738 Plant Sci., 25, 868–880, <https://doi.org/10.1016/j.tplants.2020.04.003>, 2020.



- 739 6. Cassiani, G., Boaga, J., Vanella, D., Perri, M. T., and Consoli, S.: Monitoring and modelling of soil–plant interactions:
740 the joint use of ERT, sap flow and eddy covariance data to characterize the volume of an orange tree root zone,
741 Hydrol. Earth Syst. Sci., 19, 2213–2225, <https://doi.org/10.5194/hess-19-2213-2015>, 2015.
- 742 7. Cassiani, G., Boaga, J., Rossi, M., Putti, M., Fadda, G., Majone, B., and Bellin, A.: Soil–plant interaction monitoring:
743 Small scale example of an apple orchard in Trentino, North-Eastern Italy, Science of The Total Environment, 543,
744 851–861, <https://doi.org/10.1016/j.scitotenv.2015.03.113>, 2016.
- 745 8. Collins, M., Fuentes, S., and Barlow, E.: Partial rootzone drying and deficit irrigation increase stomatal sensitivity to
746 vapour pressure deficit in anisohydric grapevines, Funct Plant Biol, 37, 129–138, 2009.
- 747 9. Consoli, S., Stagno, F., Vanella, D., Boaga, J., Cassiani, G., and Rocuzzo, G.: Partial root-zone drying irrigation in
748 orange orchards: Effects on water use and crop production characteristics, European Journal of Agronomy, 82, 190–
749 202, <https://doi.org/10.1016/j.eja.2016.11.001>, 2017.
- 750 10. Cseresnyés, I., Vozáry, E., Kabos, S., and Rajkai, K.: Influence of substrate type and properties on root electrical
751 capacitance, Int. Agrophysics, 34, 95–101, <https://doi.org/10.31545/intagr/112147>, 2020.
- 752 11. Dalton, F. N.: In-situ root extent measurements by electrical capacitance methods, Plant Soil, 173, 157–165,
753 <https://doi.org/10.1007/BF00155527>, 1995.
- 754 12. Dietrich, S., Carrera, J., Weinzettel, P., and Sierra, L.: Estimation of Specific Yield and its Variability by Electrical
755 Resistivity Tomography, Water Resour. Res., 54, 8653–8673, <https://doi.org/10.1029/2018WR022938>, 2018.
- 756 13. Doussan, C. and Garrigues, E.: Measuring and Imaging the Soil-root-water System with a Light Transmission 2D
757 Technique, Bio-Protocol, 9, <https://doi.org/10.21769/BioProtoc.3190>, 2019.
- 758 14. Düring, H., Dry, P. R., Botting, D. G., and Loveys, B.: Effects of partial root-zone drying on grapevine vigour, yield,
759 composition of fruit and use of water, in: Proceedings of the Ninth Australian Wine Industry Technical Conference :
760 Adelaide, South Australia, 16-19 july 1995, 1996, págs. 128-131, Proceedings of the Ninth Australian Wine Industry
761 Technical Conference : Adelaide, South Australia, 16-19 july 1995, 128–131, 1996.



- 762 15. Ehosioke, S., Nguyen, F., Rao, S., Kremer, T., Placencia-Gomez, E., Huisman, J. A., Kemna, A., Javaux, M., and
763 Garré, S.: Sensing the electrical properties of roots: A review, *Vadose Zone J.*, 19, e20082,
764 <https://doi.org/10.1002/vzj2.20082>, 2020.
- 765 16. Elsner, E. A. and Jubb, G. L.: Leaf Area Estimation of Concord Grape Leaves from Simple Linear Measurements,
766 *Am. J. Enol. Vitic.*, 39, 95–97, 1988.
- 767 17. Garré, S., Hyndman, D., Mary, B., and Werban, U.: Geophysics conquering new territories: The rise of
768 “agrogeophysics,” *Vadose Zone J.*, 20, e20115, <https://doi.org/10.1002/vzj2.20115>, 2021.
- 769 18. Garrigues, E., Doussan, C., and Pierret, A.: Water Uptake by Plant Roots: I – Formation and Propagation of a Water
770 Extraction Front in Mature Root Systems as Evidenced by 2D Light Transmission Imaging, *Plant Soil*, 283, 83–98,
771 <https://doi.org/10.1007/s11104-004-7903-0>, 2006.
- 772 19. Geuzaine, C. and Remacle, J.-F.: Gmsh: A 3-D finite element mesh generator with built-in pre- and post-processing
773 facilities, *Int. J. Numer. Methods Eng.*, 79, 1309–1331, <https://doi.org/10.1002/nme.2579>, 2009.
- 774 20. Gibert, D., Le Mouél, J.-L., Lambs, L., Nicollin, F., and Perrier, F.: Sap flow and daily electric potential variations in
775 a tree trunk, *Plant Science*, 171, 572–584, <https://doi.org/10.1016/j.plantsci.2006.06.012>, 2006.
- 776 21. Gimenez, C., Gallardo, M., and Thompson, R. B.: PLANT–WATER RELATIONS, in: *Encyclopedia of Soils in the*
777 *Environment*, edited by: Hillel, D., Elsevier, Oxford, 231–238, <https://doi.org/10.1016/B0-12-348530-4/00459-8>,
778 2005.
- 779 22. Gu, H., Liu, L., Butnor, J., Sun, H., Zhang, X., Li, C., and Liu, X.: Electrical capacitance estimates crop root traits
780 best under dry conditions—a case study in cotton (*Gossypium hirsutum* L.), *Plant Soil*, 467, 1–19,
781 <https://doi.org/10.1007/s11104-021-05094-6>, 2021.
- 782 23. Hoagland, D. R. and Arnon, D. I. (1950). The water culture method for growing plants without soil. *California Agric*
783 *Exp Stn Circ* 347: 1-32.
- 784 24. Jackisch, C., Knoblauch, S., Blume, T., Zehe, E., and Hassler, S. K.: Estimates of tree root water uptake from soil
785 moisture profile dynamics, *Biogeosciences*, 17, 5787–5808, <https://doi.org/10.5194/bg-17-5787-2020>, 2020.



- 786 25. Kamarajan, C., Pandey, A. K., Chorlian, D. B., and Porjesz, B.: The use of current source density as
787 electrophysiological correlates in neuropsychiatric disorders: a review of human studies, *Int. J. Psychophysiol. Off.*
788 *J. Int. Organ. Psychophysiol.*, 97, 310–322, <https://doi.org/10.1016/j.ijpsycho.2014.10.013>, 2015.
- 789 26. Liu, Y., Li, D., Qian, J., Di, B., Zhang, G., and Ren, Z.: Electrical impedance spectroscopy (EIS) in plant roots
790 research: a review, *Plant Methods*, 17, <https://doi.org/10.1186/s13007-021-00817-3>, 2021.
- 791 27. Lovisolo, C., Lavoie-Lamoureux, A., Tramontini, S., and Ferrandino, A.: Grapevine adaptations to water stress: new
792 perspectives about soil/plant interactions, *Theor. Exp. Plant Physiol.*, 28, 53–66, [https://doi.org/10.1007/s40626-016-](https://doi.org/10.1007/s40626-016-0057-7)
793 [0057-7](https://doi.org/10.1007/s40626-016-0057-7), 2016.
- 794 28. Malavasi, U. C., Davis, A. S., and Malavasi, M. de M.: Lignin in Woody Plants under Water Stress: A Review,
795 *Floresta E Ambiente*, 23, 589–597, <https://doi.org/10.1590/2179-8087.143715>, 2016.
- 796 29. Michot, D., Benderitter, Y., Dorigny, A., Nicoullaud, B., King, D., and Tabbagh, A.: Spatial and temporal monitoring
797 of soil water content with an irrigated corn crop cover using surface electrical resistivity tomography: Soil Water
798 Study Using Electrical Resistivity, *Water Resour. Res.*, 39, <https://doi.org/10.1029/2002WR001581>, 2003.
- 799 30. Mancuso, S. (Ed.): *Measuring roots: an updated approach*, Springer, Heidelberg ; New York, 382 pp., 2012.
- 800 31. Martin-Vertedor, A. I. and Dodd, I. C.: Root-to-shoot signalling when soil moisture is heterogeneous: increasing the
801 proportion of root biomass in drying soil inhibits leaf growth and increases leaf abscisic acid concentration: Root
802 distribution and non-hydraulic signalling, *Plant Cell Environ.*, 34, 1164–1175, [https://doi.org/10.1111/j.1365-](https://doi.org/10.1111/j.1365-3040.2011.02315.x)
803 [3040.2011.02315.x](https://doi.org/10.1111/j.1365-3040.2011.02315.x), 2011.
- 804 32. Mary, B., Peruzzo, L., Boaga, J., Schmutz, M., Wu, Y., Hubbard, S. S., and Cassiani, G.: Small-scale characterization
805 of vine plant root water uptake via 3-D electrical resistivity tomography and mise-à-la-masse method, *Hydrol. Earth*
806 *Syst. Sci.*, 22, 5427–5444, <https://doi.org/10.5194/hess-22-5427-2018>, 2018.
- 807 33. Mary, B., Vanella, D., Consoli, S., and Cassiani, G.: Assessing the extent of citrus trees root apparatus under deficit
808 irrigation via multi-method geo-electrical imaging, *Sci. Rep.*, 9, 9913, <https://doi.org/10.1038/s41598-019-46107-w>,
809 2019a.



- 810 34. Mary, B., Rao, S., Javaux, M., and Cassiani, G.: Tree root system mise-à-la-masse (MALM) forward modelling with
811 explicit representation of root structure., in: Geophysical Research Abstracts, 2019b.
- 812 35. McAdam, S. A. M., Sussmilch, F. C., and Brodribb, T. J.: Stomatal responses to vapour pressure deficit are regulated
813 by high speed gene expression in angiosperms, *Plant Cell Environ.*, 39, 485–491, <https://doi.org/10.1111/pce.12633>,
814 2016.
- 815 36. Parsekian, A. D., Claes, N., Singha, K., Minsley, B. J., Carr, B., Voytek, E., Harmon, R., Kass, A., Carey, A., Thayer,
816 D., and Flinchum, B.: Comparing Measurement Response and Inverted Results of Electrical Resistivity Tomography
817 Instruments, *J. Environ. Eng. Geophys.*, 22, 249–266, <https://doi.org/10.2113/JEEG22.3.249>, 2017.
- 818 37. Peruzzo, L., Chou, C., Wu, Y., Schmutz, M., Mary, B., Wagner, F. M., Petrov, P., Newman, G., Blancaflor, E. B.,
819 Liu, X., Ma, X., and Hubbard, S.: Imaging of plant current pathways for non-invasive root Phenotyping using a newly
820 developed electrical current source density approach, *Plant Soil*, 450, 567–584, [https://doi.org/10.1007/s11104-020-](https://doi.org/10.1007/s11104-020-04529-w)
821 [04529-w](https://doi.org/10.1007/s11104-020-04529-w), 2020.
- 822 38. Peruzzo, L., Liu, X., Chou, C., Blancaflor, E. B., Zhao, H., Ma, X.-F., Mary, B., Iván, V., Weigand, M., and Wu, Y.:
823 Three-channel electrical impedance spectroscopy for field-scale root phenotyping, *Plant Phenome J.*, 4, e20021,
824 <https://doi.org/10.1002/ppj2.20021>, 2021.
- 825 39. Postic, F. and Doussan, C.: Benchmarking electrical methods for rapid estimation of root biomass, *Plant Methods*,
826 12, 33, <https://doi.org/10.1186/s13007-016-0133-7>, 2016.
- 827 40. Rao, S., Meunier, F., Ehosioke, S., Lesparre, N., Kemna, A., Nguyen, F., Garré, S., and Javaux, M.: A mechanistic
828 model for electrical conduction in soil–root continuum: a virtual rhizotron study, *Biogeochemistry: Land*,
829 <https://doi.org/10.5194/bg-2018-280>, 2018.
- 830 41. Sartoni, R., Zegada-Lizarazu, W., and Monti, A.: A new compartmentalised rhizotron system for root phenotyping,
831 *Ital. J. Agron.*, 10, 53, <https://doi.org/10.4081/ija.2015.645>, 2015.
- 832 42. Sharp, R. E. and Davies, W. J.: Regulation of growth and development of plants growing with a restricted supply of
833 water, *Semin. Ser. - Soc. Exp. Biol.*, 1989.



- 834 43. Smart, D. R., Carlisle, E., Goebel, M., and Nunez, B. A.: Transverse hydraulic redistribution by a grapevine, *Plant*
835 *Cell Environ*, 28, 157–166, <https://doi.org/10.1111/j.1365-3040.2004.01254.x>, 2005.
- 836 44. Song, C., Shen, W., Du, L., Wen, J., Lin, J., and Li, R.: Development and chemical characterization of Casparian
837 strips in the roots of Chinese fir (*Cunninghamia lanceolata*), *Trees*, 33, 827–836, [https://doi.org/10.1007/s00468-019-](https://doi.org/10.1007/s00468-019-01820-x)
838 01820-x, 2019.
- 839 45. Stoll, M.: Effects of partial rootzone drying on grapevine physiology and fruit quality, 2000.
- 840 46. Stoll, M., Loveys, B., and Dry, P.: Hormonal changes induced by partial rootzone drying of irrigated grapevine,
841 *Journal of Experimental Botany*, 51, 1627–1634, <https://doi.org/10.1093/jexbot/51.350.1627>, 2000.
- 842 47. Taylor, H. M., Upchurch, D. R., and McMichael, B. L.: Applications and limitations of rhizotrons and minirhizotrons
843 for root studies, *Plant Soil*, 129, 29–35, <https://doi.org/10.1007/BF00011688>, 1990.
- 844 48. Tsialtas, J. T., Koundouras, S., and Zioziou, E.: Leaf area estimation by simple measurements and evaluation of leaf
845 area prediction models in Cabernet-Sauvignon grapevine leaves, *Photosynthetica*, 46, 452–456,
846 <https://doi.org/10.1007/s11099-008-0077-x>, 2008.
- 847 49. Tsukanov, K. and Schwartz, N.: Relationship between wheat root properties and its electrical signature using the
848 spectral induced polarization method, *Vadose zone j.*, 19, <https://doi.org/10.1002/vzj2.20014>, 2020.
- 849 50. Tsukanov, K. and Schwartz, N.: Modeling Plant Roots Spectral Induced Polarization Signature, *Geophys. Res. Lett.*,
850 48, e2020GL090184, <https://doi.org/10.1029/2020GL090184>, 2021.
- 851 51. Uhlemann, S., Wilkinson, P. B., Maurer, H., Wagner, F. M., Johnson, T. C., and Chambers, J. E.: Optimized survey
852 design for electrical resistivity tomography: combined optimization of measurement configuration and electrode
853 placement, *Geophys. J. Int.*, 214, 108–121, <https://doi.org/10.1093/gji/ggy128>, 2018.
- 854 52. Urban, J., Bequet, R., and Mainiero, R.: Assessing the applicability of the earth impedance method for in situ studies
855 of tree root systems, *J. Exp. Bot.*, 62, 1857–1869, <https://doi.org/10.1093/jxb/erq370>, 2011.
- 856 53. Vanella D., G. Cassiani, L. Busato, J. Boaga, S. Barbagallo, A. Binley, S. Consoli, 2018, Use of small scale electrical
857 resistivity tomography to identify soil-root interactions during deficit irrigation, *Journal of Hydrology*, 556, 310-324,
858 doi: 10.1016/j.jhydrol.2017.11.025.



- 859 54. Virtanen, P., Gommers, R., Oliphant, T. E., Haberland, M., Reddy, T., Cournapeau, D., Burovski, E., Peterson, P.,
860 Weckesser, W., Bright, J., van der Walt, S. J., Brett, M., Wilson, J., Millman, K. J., Mayorov, N., Nelson, A. R. J.,
861 Jones, E., Kern, R., Larson, E., Carey, C. J., Polat, İ., Feng, Y., Moore, E. W., VanderPlas, J., Laxalde, D., Perktold,
862 J., Cimrman, R., Henriksen, I., Quintero, E. A., Harris, C. R., Archibald, A. M., Ribeiro, A. H., Pedregosa, F., and
863 van Mulbregt, P.: SciPy 1.0: fundamental algorithms for scientific computing in Python, *Nat. Methods*, 17, 261–272,
864 <https://doi.org/10.1038/s41592-019-0686-2>, 2020.
- 865 55. Voytek, E. B., Barnard, H. R., Jougnot, D., and Singha, K.: Transpiration- and precipitation-induced subsurface water
866 flow observed using the self-potential method, *Hydrol. Process.*, <https://doi.org/10.1002/hyp.13453>, 2019.
- 867 56. Whalley, W. R., Binley, A., Watts, C. W., Shanahan, P., Dodd, I. C., Ober, E. S., Ashton, R. W., Webster, C. P.,
868 White, R. P., and Hawkesford, M. J.: Methods to estimate changes in soil water for phenotyping root activity in the
869 field, *Plant Soil*, 415, 407–422, <https://doi.org/10.1007/s11104-016-3161-1>, 2017.
- 870 57. Weigand, M.: *Monitoring Structural And Physiological Properties Of Crop Roots Using Spectral Electrical*
871 *Impedance Tomography*, University of Bonn, 2017.
- 872 58. Weigand, M. and Kemna, A.: Imaging and functional characterization of crop root systems using spectroscopic
873 electrical impedance measurements, *Plant Soil*, 435, 201–224, <https://doi.org/10.1007/s11104-018-3867-3>, 2019.
- 874 59. Yan, J., Bogie, N. A., and Ghezzehei, T. A.: Root uptake under mismatched distributions of water and nutrients in
875 the root zone, *Biogeosciences*, 17, 6377–6392, <https://doi.org/10.5194/bg-17-6377-2020>, 2020.